A developmentally regulated long-range enhancer-promoter contact mediates human neural development

Devin Bready[1,2], Shuai Wang[1], Niklas Ravn-Boess[1], Joshua Frenster[1], Jonathan Sabio[1], Robert Kushmakov[1], Finnegan Clark[3], Adler Guerrero[1], Cathryn Lapierre[1], Kristyn Galbraith[4], Catherine Do[4], Priscillia Lhoumaud[4], Jod Prado[1], Albert Jiang[1], Sara Haddock[1], Claire D. Kim[1], Matija Snuderl[4,5], Timothée Lionnet[3,6], Aristotelis Tsirigos[4,7,8], Jane Skok[4,5], Dimitris G. Placantonakis[1,5,6,9,10]**

[1]Department of Neurosurgery, New York University Grossman School of Medicine, NY
[2]Medical Scientist Training Program, New York University Grossman School of Medicine, NY
[3]Institute for Systems Genetics, New York University Grossman School of Medicine, NY
[4]Department of Pathology, New York University Grossman School of Medicine, NY
[5]Perlmutter Cancer Center, NYU Langone Health, NY
[6]Department of Cell Biology, New York University Grossman School of Medicine, NY
[7]Department of Medicine, New York University Grossman School of Medicine, NY
[8]Applied Bioinformatics Laboratory, New York University Grossman School of Medicine, NY
[9]Neuroscience Institute, New York University Grossman School of Medicine, NY
[10]Lead contact
**Correspondence: dimitris.placantonakis@nyulangone.org

SUMMARY

SOX2 is a core pluripotency factor in human embryonic stem cells (hESCs), but upon differentiation to the three germ layers, its expression is preserved selectively in neuroectoderm. The mechanisms regulating *SOX2* transcription in distinct developmental stages remain incompletely understood. Here, we demonstrate that a distant enhancer 550 kb from the human *SOX2* locus is selectively activated in neural stem cells (NSCs) and establishes long-range contact with the *SOX2* gene. CRISPR-Cas9 excision of the enhancer has no effect in hESCs but reduces *SOX2* transcription in NSCs and impairs neuroectodermal differentiation and forebrain specification in teratomas and cerebral organoids. CRISPR excision of a CTCF recognition motif adjacent to the enhancer does not affect enhancer activation in neuroectoderm but reduces chromatin looping and *SOX2* transcription to partially reproduce phenotypes seen with enhancer deletion. Our findings indicate that the development of the human nervous system depends on a developmentally regulated long-range contact between a distant enhancer and the *SOX2* locus.

KEYWORDS

SOX2, enhancer, CTCF, chromatin organization, neuroectoderm, forebrain, gene regulation, development

INTRODUCTION

Embryonic development relies on spatiotemporally orchestrated lineage commitment and differentiation steps that start with pluripotent stem cells (PSCs) in the inner cell mass and lead to the full gamut of cell fates that populate the embryo. Each one of these steps requires lineage-defining transcriptional programs, which are determined by specific transcription factors (TFs) and epigenetic mechanisms[1,2] that include both coding and non-coding regions of the genome. Within the non-coding genome, enhancers are regulatory elements that can influence transcription at target loci at a distance through interactions mediated by three-dimensional (3D) chromatin folding. One tier of 3D chromatin organization involves topologically associating domains (TADs), which are 0.5-1.0 Mb-long chromatin loops that facilitate intra-loop 3D contacts[3,4] and whose formation relies on the cohesin complex and DNA-binding chromatin organizer CTCF.[5,6] The dynamic regulation of TAD organization and 3D chromatin contacts in normal development and disease is an area of active investigation.[7]

SOX2 belongs to the SOX (SRY-related high-mobility group box) family of TFs, which includes 20 separate SOX proteins classified into 9 subfamilies.[8] Within the SOXB1 subfamily, SOX2 serves as a core pluripotency TF alongside OCT4 and NANOG in embryonic stem cells (ESCs).[9,10,11] These core pluripotency TFs support transcription of each other by forming heteromultimers in a positive-feedback mechanism,[12,13] and define a global transcriptome favoring pluripotency and preventing differentiation. Interestingly, SOX2 retains an important functional role after exit from the ESC stage. In embryogenesis, the specification of the three germ layers requires that SOX2 persist only in neuroectodermal progenitors, where it is essential for neural development.[14,15] In contrast, *SOX2* transcription is silenced in early mesodermal and endodermal lineages, with subsequent expression in endodermal lineages of the developing lung, trachea, stomach, and esophagus.[15-17] In the neural tube, SOX2 is ubiquitously expressed in the absence of other pluripotency TFs, and is required for the self-renewal and multipotency of neural progenitors.[18-24] It partners with other lineage-specific transcription factors, such as PAX6, to transactivate relevant sets of genes that define neural stem cells (NSCs),[25,26] and helps maintain bivalent chromatin marks on neuronal differentiation genes, thereby keeping them poised and readily activated when neuronal differentiation programs are initiated.[18-23] This raises the question of how *SOX2* transcription is regulated in neural progenitors relative to ESCs, given the absence of other pluripotency factors in the neural lineage. Furthermore, SOX2 is also expressed and functionally relevant in tumors deriving from neural tissue, such as glioma.[27-29] These findings underscore the importance of characterizing transcriptional regulatory mechanisms for SOX2, a gene critical to pluripotency, central nervous system development and tumorigenesis.

Previous work has characterized enhancer elements that regulate *SOX2* transcription in the mammalian nervous system, primarily using mouse models.[30-35] However, the organization of the genome around the *SOX2* locus in human central nervous system development remains incompletely understood. Here we show that, in human neural progenitors, *SOX2* transcription depends on a long-range contact with a distant enhancer located ~550 kb away within the same TAD. Activation of the enhancer and establishment of the long-range contact with the *SOX2* locus are developmentally regulated and established selectively in neural progenitors but not in human ESCs (hESCs). CRISPR-mediated excision of the enhancer does not affect hESC self-renewal, but results in impaired neural development and neurogenesis, particularly regarding the generation of forebrain lineages. Our study complements previous work on the regulation of *SOX2* transcription, but also demonstrates a developmentally regulated distant enhancer and 3D chromatin loop crucial to neural and forebrain development.[32,36,37] This mechanism highlights the impact of dynamic reconfiguration of the non-coding genome and 3D organization of chromatin during development.

RESULTS

A phylogenetically conserved and neuroectoderm-specific long-range contact between a distant enhancer and the human SOX2 locus

Our previous work suggested that, in hESC-derived NSCs, the *SOX2* gene locus in chromosome 3q makes a strong long-range contact with a region ~550 kb telomeric to it within the canonical TAD of this genomic neighborhood in 4C-seq assays[38] (Figure 1A). This region is marked by a CTCF cognate motif (numbered 5 and termed *nMotif* hereafter), while the *SOX2* locus is also marked by several CTCF motifs (numbered 1-4) (Figure 1A). Our Assay for Transposase-Accessible Chromatin sequencing (ATAC-seq) analysis indicated that, immediately centromeric (~16 kb) to *nMotif* lies a ~5.6 kb genomic region with the most accessible chromatin in the TAD besides the *SOX2* locus (Figure 1A). In addition, chromatin immunoprecipitation sequencing (ChIP-seq) showed that this region is highly decorated with the euchromatic histone modification H3K27ac (acetylation) but lacks the facultative repressive modification H3K27me3 (trimethylation) (Figure 1A), suggesting it may represent a transcriptionally active enhancer element. Analysis with HiC and virtual 4C validated this chromatin loop in NSCs (Figure 1B), and ChIP-seq for CTCF demonstrated CTCF occupancy at *nMotif*, as well as around the *SOX2* gene locus (Figure 1B) in NSCs.

We then tested whether this putative enhancer-promoter interaction may be relevant in other cell lineages. We interrogated data from the Epigenome Roadmap in hESCs,[39] which also express *SOX2*, and mesodermal progenitors,[40] which do not. While both NSCs and hESCs robustly transcribe *SOX2*, the enhancer has an open chromatin conformation on ATAC-seq and is decorated with the euchromatic modification H3K27ac in ChIP-seq analysis only in NSCs, but not hESCs (Figure 1B, Figure S1A). Similarly, analysis of HiC data with virtual 4C, utilizing either the *SOX2* genomic locus or the distant enhancer as the viewpoint, indicated that the long-range contact is significantly more prominent in NSCs than hESCs (Figure 1B, Figure S1B). We found no evidence for enhancer activation or chromatin looping in public domain ChIP-seq and HiC from mesodermal progenitors,[40] which do not express *SOX2* (Figure S1A,B). These data suggested the developmental co-regulation of this enhancer and the associated chromatin loop upon neuralization.

Within the genomic region corresponding to this putative enhancer lie two H3K27ac peaks, one of which was previously designated *HS1332* in the VISTA Enhancer dataset[41] (we will refer to the other peak as *HS1332b* hereafter). Further analysis suggested that the genomic sequence of this enhancer element, particularly *HS1332*, is phylogenetically conserved from zebrafish to humans (Figure 1C). Strikingly, when the vertebrate conservation scores are aligned against ChIP-Seq and ATAC-Seq of NSCs, the loci displaying the highest amount of H3K27ac are those corresponding to the conserved regions (Figure 1C).

The evolutionary conservation of the enhancer sequence itself led us to ask if the same phenomenon of TAD reorganization and putative enhancer activation could be seen during neuralization in other species. In mice, the analogous enhancer is approximately 450 kb telomeric to *SOX2* and displays a robust degree of conservation (Figure 1C,D). As in humans, while the long-range contact was absent and the enhancer was silent in mouse ECSs, upon neuralization the long-range contact surrounding the enhancer and the activation of the distal enhancer itself were robust (Figure 1D). While relevant datasets in zebrafish were sparse, we found evidence that the evolutionarily conserved enhancer element, which in the zebrafish genome is approximately 45 kb distal to *SOX2*, is also activated and recruited in embryonic brain tissue but not muscle (Figure S1C).[42] Collectively, these data lead us to hypothesize that this conserved enhancer element acts on the *SOX2* gene locus via a CTCF-mediated long-range chromatin loop to support *SOX2* transcription specifically in embryonic neural development but not in the pluripotent state (Figure 1E).

Excision of the distant enhancer or disruption of the chromatin loop impair specification of neuroectodermal lineages

To mechanistically investigate the role the long-range enhancer-*SOX2* contact plays in human development, we used a dual gRNA CRISPR-Cas9 approach to excise the 2.7 kb *HS1332* enhancer element (Δ*HS1332*) in H9 hESCs transgenic for the *Hes5::GFP* bacterial artificial chromosome (BAC)[43-45] (Figure 2A). This transgene allows identification of neural progenitors through expression of GFP. We implemented the same approach to excise the CTCF motif (90 bp) adjacent to the enhancer (Δ*nMotif*) (Figure 2A). A single gRNA targeting the human *ROSA26* locus was used as control. hESCs were transduced with lentiviruses expressing Cas9 and each respective gRNA combination and pools of cells

were isolated by FACS. To generate hESC clones with the desired genetic alterations, the FACS-isolated hESCs were plated on mouse embryonic fibroblasts (MEFs) in 24-well tissue culture plates at a nominal seeding density of 5 cells/well, which was experimentally determined to yield one clone per 24 wells seeded. Deletions in each condition were genotyped with PCR and Sanger sequencing (Figure 2B, Figure S2A). In anticipation of a lower efficiency in genome editing when excising the large *HS1332* element, further subcloning was performed. Among five further subclones generated, one was found to have the desired deletion by PCR and Sanger sequencing (Figure 2B, Figure S2A).

One clone from each of the Δ*HS1332* and Δ*nMotif* conditions was chosen for further experimentation. To confirm the deletions, we performed bulk whole genome sequencing (WGS) of hESCs from the Δ*HS1332* and Δ*nMotif* clones (Figure S2B,C), which demonstrated homozygous deletion of *nMotif* but deletion of only one of the two *HS1332* alleles. To further investigate the Δ*HS1332* condition, we generated a panel of fluorescence *in situ* hybridization (FISH) probes against the 2.7 kb deleted region of the *HS1332* enhancer and a nearby 45 kb region (~300 kb telomeric), which was not targeted for deletion (Figure S3A). A universal anchor control probe set targeting a 20 kb locus near the *HBB* (hemoglobin subunit beta) gene on chromosome 11, with known labeling efficacy, was included as an additional control. The *HS1332* probe set was expected to have low labeling efficiency given the small size of the genomic region interrogated (2.7kb). While ~70% of *ROSA26* hESCs and hESC-derived rosette neuroectodermal stem cell (rosette) cultures, which developmentally resemble neural plate precursors,[46,47] manifested *HS1332* FISH labeling, only ~30-40% of their Δ*HS1332* counterparts showed *HS1332* labeling (Figure S3B-E). Collectively, these data suggested homozygous deletion of Δ*nMotif* and hemizygous deletion of *HS1332*. A less likely possibility is that the Δ*HS1332* condition represents a mix of cells with homozygous *HS1332* deletion and wild-type cells. Finally, we utilized WGS data to generate pseudo-karyotypes that demonstrated no significant differences in chromosomal integrity among the Δ*HS1332*, Δ*nMotif* and *ROSA26* conditions (Figure S4).

Hemizygous excision of the enhancer or homozygous deletion of the nMotif had no impact on the self-renewal of hESCs, as evidenced by expression of pluripotency transcription factors (OCT4, NANOG, SOX2) and cell surface markers (SSEA4, TRA-1-81) (Figure 2C, Figure S5A,B). To assess the effects of these modifications in neural differentiation, we performed two types of assays. First, we employed *in vitro* unbiased differentiation of Δ*HS1332* or Δ*nMotif* hESCs as serum-free embryoid bodies (SFEBs).[44,45] These assays indicated significant impairment in generation of GFP+ neuroectodermal precursors derived from Δ*HS1332* or Δ*nMotif* hESCs relative to the *ROSA26* control (Figure 2D). Second, we used dual SMAD inhibition to direct differentiation of hESCs to neural rosettes.[46,47] These assays also demonstrated significant decreases in both the number of GFP+ progenitors and the intensity of GFP fluorescence in the Δ*HS1332* condition, but no significant effect in the Δ*nMotif* condition (Figure 2E). These findings suggested that perturbing the enhancer and long-range chromatin loop had no effect on hESC self-renewal but impaired specification of neuro-ectoderm.

In both excision groups, impaired neural specification correlated with significant reductions in *SOX2* transcript levels in rosettes, while no differences were observed at the hESC stage (Figure 2F). Immunoblotting for SOX2 confirmed that SOX2 protein levels were reduced at the rosette stage in the Δ*HS1332* and Δ*nMotif* conditions, with no differences seen at the hESC stage (Figure 2G). Directed neuroglial differentiation of the *SOX2*-deficient Δ*HS1332* and Δ*nMotif* rosette progenitors reproducibly failed to generate neurons, while generation of astrocytes was facilitated, as evidenced by immunostaining for beta-tubulin III (TUJ1; neuronal) and glial fibrillary acidic protein (GFAP; astrocytic), and qRT-PCR for *RBFOX3* (neuronal) and *SLC1A2* (astrocytic) mRNA (Figure 2H-J). Collectively, these data suggest that perturbation of the long-range enhancer-*SOX2* locus contact interferes with the development of neuroectodermal progenitors and subsequent neuroglial differentiation.

To validate these *in vitro* findings in an *in vivo* setting, we performed teratoma assays in NOD.Cg-*Prkdc*^{scid} *Il2r*γ^{tm1Wjl}/SzJ (NSG) mice by implanting *ROSA26,* Δ*HS1332*, and Δ*nMotif* hESCs in the flank. Teratomas can serve as a model for studying development because they recapitulate a large number of diverse cell types, including distinct neural lineages.[48] After allowing teratomas to form for six weeks (Figure 3A), we extracted them and performed blinded histologic analysis of hematoxylin and eosin (H&E) sections. This assay indicated impairment in neuroectodermal rosette formation in Δ*HS1332* and Δ*nMotif* teratomas (Figure S6A,B). Immunofluorescence microscopy of the teratomas revealed a significantly reduced prevalence of nuclei positive for SOX2 and the neuroectodermal TF PAX6 in the excision groups. Interestingly, Δ*HS1332* teratomas, and to a lesser extent Δ*nMotif* teratomas, showed enrichment for the

endodermal TF HNF3B, while no differences were found for the mesodermal marker smooth muscle actin (SMA) (Figure 3B,C).

To assess cell fates within teratomas from the *ROSA26*, Δ*HS1332* and Δ*nMotif* conditions in more detail, we carried out single-cell (single nucleus) RNA-seq (scRNA-seq) analysis. The analysis included 11958 cells in ROSA26, 5636 cells in Δ*HS1332*, and 6108 cells in Δ*nMotif* groups passing quality controls (Figure 3D). Utilizing a prior teratoma scRNA-seq dataset encompassing 179,632 cells[48] as a reference atlas, we identified 15 independent cell clusters encompassing all three germ layers. The teratomas generated from Δ*HS1332* hESC cells contained 39% ectodermal cells compared to 62% and 61% in the *ROSA26* and Δ*nMotif* conditions respectively (Figure 3E). These findings suggested that deleting the enhancer impaired neuroectodermal development with a concomitant increase in endodermal lineages.

Impaired Forebrain Specification

While the Δ*HS1332* condition produced a lower proportion of ectodermal tissues as evidenced by immunofluorescence (Figure 3B), H&E staining (Figure S6A,B), and by scRNA-seq (Figure 3E), there remained a substantial neuroectodermal population. To identify differences within neuroectodermal lineages, we extracted the cells within the ectodermal populations of each condition from the scRNA-seq dataset, and subsequently reclustered them into ten distinct clusters comprising multiple neuronal and glial cell types (Figure 3F). We then compared the Δ*HS1332 and* Δ*nMotif* neuroectoderm to that of the *ROSA26* condition with Gene Ontology (GO) analysis using ShinyGO (Figure 4A). The major GO terms that dropped out in the Δ*HS1332* condition related to axonal development, neurogenesis and forebrain development, while in the Δ*nMotif* condition the majority of depleted GO terms related to synaptic organization and axon development[49] (Figure 4A). In line with the depletion of GO terms relating to forebrain development, the forebrain transcription factors *FOXG1*[50,51] and *EMX2*[52,53] were depleted in forebrain progenitors from Δ*HS1332* and Δ*nMotif* teratomas (Figure 4B). These findings suggest that the *HS1332* enhancer and the associated chromatin loop are critical to neuralization, and particularly impactful on forebrain development.

To further investigate the forebrain phenotype observed in teratoma formation assays, hESCs were differentiated to rosettes using dual SMAD inhibition.[54] Immunofluorescent staining and imaging of Δ*HS1332* rosettes demonstrated a near complete lack of FOXG1 immunostaining (Figure 4C), confirming the findings in teratomas.

To collect additional evidence for the forebrain phenotype, we tested the function of the enhancer in cerebral organoids[55-58] from *ROSA26*, Δ*HS1332* and Δ*nMotif* hESCs (Figure 4D). Organoids were analyzed at the 30 and 40-day time-points. Immunostaining for SOX2 and GFP, from the *Hes5::GFP* reporter, were significantly reduced in the Δ*HS1332* and Δ*nMotif* conditions at 30 days, but present in the *ROSA26* condition. TUJ1 and RBFOX3 (NeuN)-positive neuronal fates were significantly reduced in the Δ*HS1332* and Δ*nMotif* conditions at both time-points (Figure 4E). Furthermore, immunostaining for forebrain transcription factors FOXG1 and EMX1 showed depletion in ΔHS1332 organoids, and in Δ*nMotif* organoids to a lesser extent. These observations support the hypothesis that the distant *SOX2* enhancer, and the associated 3D chromatin loop to a lesser extent, are particularly crucial to telencephalic development.

HS1332 Enhancer Activation does not depend on Chromatin Conformation changes

The fact that activation of the enhancer and formation of the chromatin loop within the *SOX2* TAD are developmentally co-regulated and specific to neuroectodermal fates raises the possibility of causality linking the two processes. To answer this question, we performed ChIP-seq for the activating chromatin modification H3K27ac and the facultative repressive modification H3K27me3, as well as 4C using a bait in the *SOX2* promoter, in hESCs and rosettes. In hESCs from all conditions, the enhancer element was neither activated nor repressed (Figure 5A,B), but in the Δ*HS1332* condition the *SOX2* TAD had overall diminished H3K27ac deposition and a locus centromeric to *HS1332* was heavily decorated with the H3K27me3 modification (peak 1 in Figure 5B and Figure S6C). At the rosette stage, both the control *ROSA26* condition and the Δ*HS1332* and Δ*nMotif* conditions showed decoration of the enhancer element with the activating H3K27ac modification and lack of the repressive H3K27me3 mark (Figure 5A,B). Interestingly, the *SOX2* TAD harbored increased H3K27me3 in the rosettes of the Δ*HS1332* condition at two loci telomeric to the enhancer (peaks 2 and 3 in Figure 5B and Figure S6C). Peak 2 in Figure 5B localizes in the immediate vicinity of the long non-coding RNA *LINC01994*.[34] 4C-seq detected little long-range contact between the enhancer region and the *SOX2* promoter in all hESCs. In contrast, the robust long-range contact seen in

ROSA26 rosettes was significantly diminished in the Δ*nMotif* condition (Figure 5C,D). Collectively, these data suggest that enhancer activation is not coupled to establishment of the chromatin loop, since it is observed in both the *ROSA26* and Δ*nMotif* conditions, and that the enhancer regulates activating and repressive epigenetic modifications in the *SOX2* TAD.

Disruption of the chromatin loop after NSC specification replicates SOX2 expression changes and differentiation

The experiments above tested effects of perturbing enhancer activation and chromatin looping during specification of neuroectoderm. We next tested the importance of this 3D chromatin organization in already specified human NSCs. We established cultures of hESC-derived NSCs in epidermal growth factor (EGF) and fibroblast growth factor 2 (FGF2)-containing medium and then excised the CTCF *nMotif* using a dual gRNA CRISPR-Cas9 approach. A NSC line expressing a non-targeting (NT) gRNA was used as control. Excision of the targeted motif (90 bp) was verified by PCR amplification and Sanger sequencing of the resulting product (Figure 6A). Excision of the motif decreased *SOX2* transcript levels and impacted the growth and viability of NSC cultures (Figure 6B-D). Most importantly, abrogation of this chromatin loop prevented NSC differentiation to neurons and facilitated differentiation to astrocytes (Figure 6E,F). These findings suggested a critical function for 3D chromatin organization in this TAD in *SOX2* transcription, NSC multipotency and neuroglial differentiation.

The relevance of this chromatin loop and enhancer-promoter contact to neuroglial specification was corroborated by analysis of PsychEncode ATAC-seq and H3K27ac data from postmortem adult dorsolateral prefrontal cortex (DLPFC).[59] Our analysis showed that, while both neurons (NeuN+) and glia (NeuN-) retained the chromatin loop apposing the enhancer and *SOX2* locus, the two lineages exhibited differential chromatin accessibility and euchromatic modifications (Figure 6G,H).[59,60] Indeed, NeuN- glial lineages showed greater chromatin accessibility within the *SOX2* TAD, with both the *SOX2* gene locus and the *HS1332* enhancer bearing more H3K27ac euchromatic modifications than NeuN+ neuronal lineages, a finding that may be related to reported persistence of *SOX2* expression in classes of adult astrocytes.[61] These findings support a model in which the chromatin loop is required for NSCs to generate neuroglial progeny, and also retained in the progeny despite differences in chromatin state between neuronal and glial cells.

DISCUSSION

Differentiation requires dynamic control of gene expression, for which enhancer recruitment is a core determinant.[11,62,63] The recruitment of enhancers is frequently associated with the induction of genes that are quiescent in prior development stages, thus ascribing to them important functions during developmental transitions. Understanding the activity of these regulatory mechanisms can aid in dissecting their role in development and in improving the efficiency of directed stem cell differentiation to specific lineages for research and therapeutic purposes.

SOX2, alongside OCT4 and NANOG, form a core pluripotency TF network in ESCs that acts to sustain transcription of all three genes, while also maintaining pluripotency and suppressing differentiation programs.[9,10,12,13] In the developing nervous system, however, where OCT4 and NANOG are absent, *SOX2* transcription is maintained via reliance on other incompletely understood mechanisms, including other TFs and enhancer elements.[64-66] The importance and functional roles of such neuroectodermal enhancers acting on *SOX2* have only been partially explored.[32,33,37]

This study points to the importance of dynamic reconfiguration of chromatin organization during development. Within the TAD where *SOX2* resides, the chromatin landscape undergoes significant changes during the specification of neuroectoderm. We discovered that in hESCs the *SOX2* locus does not form strong 3D contacts with other elements within the TAD and the *HS1332* enhancer is silent but not repressed, as suggested by lack of facultative repressive H3K27me3 modifications. Upon differentiation to neuroectodermal stem cell fates, however, *HS1332* and the neighboring *HS1132b* loci are decorated with euchromatic activating H3K27ac modifications and a 3D chromatin loop with the *SOX2* gene is established, likely mediated by CTCF binding to motifs adjacent to the enhancer and the gene. Perturbation of the enhancer or its 3D contact with the *SOX2* gene impairs the formation of neuroectoderm, and the forebrain in particular. Mechanistically, the establishment of the 3D contact and the activation of the enhancer occur independently of each other even though they coincide spatiotemporally during neural development. This is evidenced by the finding that the enhancer still manifests activating chromatin modifications when the 3D chromatin loop is disrupted by excision of the adjacent CTCF motif.

Multiple lines of evidence suggest that this coordinated activation of the enhancer and the chromatin loop in neural lineages are crucial developmental events. First, the genomic sequences representing the enhancer are highly conserved from fish to primates. Second, the enhancer element manifests the highest amount of euchromatic modifications within the *SOX2* TAD in neuroectoderm besides the *SOX2* gene. Third, the 3D contact between the *SOX2* locus and enhancer is the strongest within the TAD and highly conserved in evolution. Finally, this 3D chromatin architecture is preserved in mature neuronal and glial lineages in the human brain, indicating either “imprinting” or a lasting functional role for it after neuroglial differentiation. Collectively, these observations suggest that this developmentally co-regulated enhancer activation and contact with the *SOX2* gene is an evolutionarily ancient mechanism essential to neuroectodermal development and neuroglial specification. This hypothesis received strong support from our perturbation experiments.

Our data suggest a role for this 3D interaction not only during developmental transitions from pluripotency to neuroectodermal fates, but also after establishment of the neural lineage. Indeed, ablation of the CTCF motif adjacent to the enhancer in NSCs prevented their differentiation to neurons, a central property of NSC multipotency. This finding, along with the observation that this 3D loop and the TAD topology are preserved in mature neurons and glia, suggest that enhancer-promoter interactions and 3D chromatin architecture do not just govern specification of stem cells, but are also critical in the maintenance of stem cell states.

Of particular interest is the finding that hemizygous deletion of the enhancer produced stronger phenotypes than homozygous deletion of the CTCF motif responsible for the 3D contact between the *SOX2* gene and the enhancer. Although our 4C sequencing showed that deletion of the particular CTCF motif substantially reduced the strength of the related chromatin loop, it is possible that the residual infrequent 3D contact suffices for the enhancer to elicit effects on *SOX2* transcriptional regulation via a “kiss-and-run” mechanism[67]. An alternative explanation is that this enhancer regulates multiple elements within the TAD beyond just the *SOX2* gene. Consistent with this theory is the fact that deletion of the enhancer results in repression of other non-coding sequences within the *SOX2* TAD (peaks 2 and 3 in Figure 5B), including long non-coding RNAs.[34]

The reason that we were able to achieve only a hemizygous but not a homozygous deletion of the *HS1332* is unclear. The size of the genomic sequence targeted for deletion, 2.7 kb, may be a contributing factor in reducing efficacy of the excision. Alternatively, it is possible that homozygous deletion of the enhancer is deleterious to hESCs. Aligned with this hypothesis is the observation that, while our assays indicated no effects of the hemizygous *HS1332* deletion on hESC self-renewal and pluripotency markers, our ChIP-sequencing revealed increased H3K27me3 deposition in a non-coding sequence in the *SOX2* TAD (peak 1 in Figure 5B) at the hESC stage. Collectively, these observations raise the possibility that the *HS1332* enhancer may exert effects on several sequences within the *SOX2* TAD besides the *SOX2* gene itself in both neuroectodermal lineages and potentially hESCs as well.

The essentiality of SOX2 to the development of the central nervous system, and neurons in particular, has been documented both experimentally and with human genetic studies. In our hands, SOX2 haploinsufficiency arising from *HS1332* deletion or excision of the adjacent CTCF motif resulted in impaired specification of neural progenitors and a profound decrease in neuronal differentiation. Our findings are in line with previous mouse models showing that neural progenitors with *SOX2* hypomorphic genetic alterations produce neurons less efficiently,[18,19] and with clinical data from patients with *SOX2* haploinsufficiency leading to anophthalmia or microphthalmia, brain malformations and learning disabilities, as well as esophageal, genital and endocrinologic developmental abnormalities.[68-70] Similarly, haploinsufficiency of *FOXG1*, a TF critical to forebrain development[51] whose expression is significantly reduced in our hands after deletion of the *HS1332* enhancer or perturbation of the associated chromatin loop, is associated with brain malformation, microcephaly, mental retardation and Rett syndrome.[68,71]

Our work has important implications for human stem cell and regenerative biology. Understanding the complex genomic mechanisms that govern developmental transitions in humans is crucial to improving protocols for directed differentiation from existing stem cell platforms. As an example of the translational utility of our findings, one could test whether direct activation of the enhancer element facilitates the generation of human neurons with a forebrain identity. Of equal interest and translational potential is the fact that SOX2 is expressed in tumors deriving from tissues whose development depends on SOX2, such as glioma, lung, and esophageal adenocarcinoma.[27-29,34] Examining how enhancers such as the one we investigated function in the context of cancer may shed light on the oncologic regulation of *SOX2* expression and offer targets for therapy.

RESOURCE AVAILABILITY

Lead contact

Further information and requests for resources and reagents should be directed to and will be fulfilled by the lead contact, Dimitris G. Placantonakis (Dimitris.placantonakis@nyulangone.org).

Materials availability

Cell lines are available upon request.

Data and code availability

- Single-cell RNA-seq, ChIP-seq, ATAC-seq, HiC, and 4C-seq data have been deposited at GEO (accession number pending) and will be publicly available when the manuscript is published.
- Any additional information required to reanalyze the data reported in this paper is available from the lead contact upon request.

ACKNOWLEDGMENTS

This work was supported by NIH R01NS124920 (DGP), NYSTEM (NY State Stem Cell Science) IIRP C32595GG (DGP), NIH R01NS102665 (DGP), NIH R21NS126806 (DGP), NIH F30CA247418 (DB), NIH R35GM122515 (JS), NIH P01CA229086 (JS), NIH R01AG075272 (TL), NIH R01CA260028 (TL), and NIH P30CA016087 (NYU Perlmutter Cancer Center Support Grant). We acknowledge the PsychEncode Consortium for sharing data from human brain specimens.

AUTHOR CONTRIBUTIONS

Conceptualization, DB and DGP; methodology, DB, JS, DGP; investigation, all authors; writing—original draft, DB and DGP; writing—review & editing, all authors; funding acquisition, DB, DGP; resources, MS, TL, AS, JS, DGP; supervision, DGP.

DECLARATION OF INTERESTS

DGP has received consultant fees from Tocagen, Synaptive Medical, Monteris, Robeaute, Advantis, and Servier Pharmaceuticals in the past, all unrelated to the presented work. DGP is listed as inventor on patents related to glioblastoma therapies, unrelated to the presented work.

DECLARATION OF GENERATIVE AI AND AI-ASSISTED TECHNOLOGIES

While preparing this work, the author(s) did not utilize any generative AI or AI-assisted technologies.

SUPPLEMENTAL INFORMATION

Figure S1. 3D chromatin organization and chromatin modifications within the *SOX2* TAD in distinct developmental stages and tissues
Figure S2. Genotyping and Whole Genome Sequencing (WGS) for Δ*HS1332* and Δ*nMotif* hESCs
Figure S3. FISH analysis in ΔHS1332 hESCs and rosettes
Figure S4. WGS-inferred pseudo-karyotypes in hESCs
Figure S5. Flow cytometric assessment of pluripotency cell surface markers
Figure S6. H&E staining of teratomas and quantification of repressive chromatin modifications in loci within the *SOX2* TAD

404 **FIGURE TITLES AND LEGENDS**

405 **Figure 1. A conserved and neuroectoderm-specific long-range contact between a distant enhancer**
406 **and the *SOX2* locus.**

407 (A) Genomic organization of a 1 Mb domain of the *SOX2* TAD in human NSCs. 4C-sequencing with a
408 *SOX2* bait, ATAC-Sequencing, and H3K27ac and H3K27me3 ChIP-sequencing are shown.
409 (B) Comparison of hESC and NSC HiC sequencing, ChIP-sequencing for CTCF, H3K27ac, and
410 H3K27me3, RNA-sequencing transcript reads, and virtual 4C-Sequencing visualizations (derived
411 from HiC sequencing) with a viewpoint of either the *SOX2* gene promoter or the putative enhancer
412 region. See also Figure S1A,B.
413 (C) Genome browser view of *HS1332* and adjacent *HS1332b* sequences corresponding to the putative
414 enhancer in the human genome with H3K27ac ChIP-sequencing and ATAC-sequencing from
415 NSCs, PhyloP score for 100 vertebrate genomes, and view of conserved sequences (green bars)
416 for 6 select species. See also Figure S1C.
417 (D) Comparison of mouse ESC and NSC HiC sequencing, ChIP-sequencing for CTCF, H3K27ac, and
418 H3K27me3, and virtual 4C-Sequencing visualizations (derived from HiC sequencing) with a
419 viewpoint of either the *SOX2* gene promoter or the putative enhancer region.
420 (E) Schematic demonstrating the hypothesis tested.

421

422 **Figure 2. Disruption of *HS1332* and the associated 3D chromatin loop impair neuralization, SOX2**
423 **expression and neuronal differentiation**

424 (A) Graphical representation of targeted deletion of either the *HS1332* enhancer or the CTCF *nMotif*.
425 (B) Gel electrophoresis of PCR products of the *HS1332*-containing domain in *ROSA26* vs Δ*HS1332*
426 hESCs (top), or the *nMotif*-containing domain in *ROSA26* vs Δ*nMotif* hESCs (bottom). Additional
427 information is found in Figures S2, S3.
428 (C) Representative immunofluorescence images for hESC markers SOX2 (red), OCT4 (green), Nanog
429 (teal) across the *ROSA26*, Δ*HS1332*, and Δ*nMotif* conditions at the hESC stage. Nuclei were
430 counterstained with DAPI.
431 (D) Graphical representation of embryoid body (SFEB) formation experiments highlighting the
432 emergence of GFP expression from the *Hes5::GFP* reporter (top). Representative images from
433 *ROSA26*, Δ*HS1332*, and Δn*Motif* SFEBs (bottom left). The bar graph (bottom right) represents the
434 quantification of GFP-positive SFEBs (n=3 biological replicates, one-way ANOVA $F_{2,6}$=13.43, p
435 <0.01; Tukey's *post hoc* multiple comparison test: *ROSA26* vs Δ*HS1332* **p<0.01; *ROSA26* vs
436 Δ*nMotif* *p<0.05).
437 (E) Graphical representation of directed *in vitro* differentiation to neural rosettes (top) and
438 representative wide field fluorescence images of each line (bottom left). The bar graph in the middle
439 shows quantification of the percentage of GFP-positive (GFP+) cells after directed differentiation
440 as measured via flow cytometry, normalized to the *ROSA26* condition in each biological replicate
441 (n=6 biological replicates, one-way ANOVA $F_{2,15}$=10.76, p=0.0013; Tukey's *post hoc* multiple
442 comparison test: *ROSA26* vs Δ*HS1332* **p<0.01). ns, not significant. The bar graph on the right
443 shows mean GFP intensity in rosettes across experimental conditions (n=6 biological replicates,
444 one-way ANOVA $F_{2,9}$=5.921, p=0.0228; Tukey's *post hoc* multiple comparison test: *ROSA26* vs
445 Δ*HS1332* **p<0.01). ns, not significant.
446 (F) qRT-PCR analysis shows no change in *SOX2* transcript levels at the hESC stage (n = 3 biological
447 replicates, one-way ANOVA $F_{2,7}$=0.1535, p=0.8605) and a decrease in *SOX2* transcript in
448 Δ*HS1332* and Δn*Motif* rosettes (n=4 biological replicates, ANOVA $F_{2,6}$=11.11, p=0.0096; Tukey's
449 *post hoc* multiple comparison test: *ROSA26* vs Δ*HS1332* *p < 0.05, *ROSA26* vs Δ*nMotif* *p < 0.05).
450 ns, not significant.
451 (G) Representative immunoblots for SOX2 and β-Actin show SOX2 downregulation in rosettes but not
452 hESCs in the Δ*HS1332* and Δn*Motif* conditions (left). Bar graphs (right) demonstrate summary
453 densitometry statistics for hESCs (n=7 biological replicates, one-way ANOVA $F_{2,18}$=0.1062,
454 p=0.8998; Tukey's *post hoc* multiple comparison test: *ROSA26* vs Δ*HS1332* p>0.05; *ROSA26* vs
455 Δ*nMotif* p>0.05) and rosettes (n=6 biological replicates, one-way ANOVA $F_{2,15}$=11.10, p=0.0011;

Tukey's *post hoc* multiple comparison test: *ROSA26* vs ΔHS1332 *p<0.05, *ROSA26* vs Δ*nMotif* ***p<0.001). ns, not significant.

(H) Immunofluorescence microscopy before and after differentiation of rosettes to neurons (left) and astrocytes (right).

(I) qRT-PCR for *RBFOX3* transcript normalized to *GAPDH* following 2 weeks of neuronal differentiation with BDNF and ascorbic acid (n=4 biological replicates, one-way ANOVA $F_{2,8}$=8.999, p<0.01; Tukey's *post hoc* multiple comparison test: *ROSA26* vs Δ*HS1332* *p < 0.05, *ROSA26* vs Δ*nMotif* *p < 0.05).

(J) qRT-PCR for *SLC1A2* transcript normalized to *GAPDH* following 2 weeks of astrocytic differentiation with 4% FBS (n=4 biological replicates, one-way ANOVA $F_{2,8}$=7.469, p=0.0104; Tukey's *post hoc* multiple comparison test: *ROSA26* vs Δ*HS1332* *p<0.05, *ROSA26* vs Δ*nMotif* *p<0.05).

Figure 3. Loss of *HS1332* or CTCF-mediated 3D organization of the TAD impairs neuroectodermal development in teratomas

(A) Graphical representation of teratoma formation experiments.

(B) Immunofluorescence microscopic analysis of *ROSA26*, Δ*HS1332*, and Δ*nMotif* teratomas harvested after 6 weeks. Representative images are shown for GFP, SOX2, PAX6, HNF3B, and smooth muscle actin (SMA).

(C) Quantification of teratoma immunofluorescence markers: GFP (n=4 biological replicates, one-way ANOVA $F_{2,8}$=28.84, p=0.0002; Tukey's *post hoc* multiple comparison test: *ROSA26* vs Δ*HS1332* **p < 0.01, *ROSA26* vs Δ*nMotif* ***p < 0.001); PAX6 (n=5 biological replicates, ANOVA $F_{2,13}$= 6.030, p=0.0140, Tukey's *post hoc* multiple comparison test: *ROSA26* vs Δ*HS1332* *p<0.05, *ROSA26* vs Δ*nMotif* *p<0.05); SOX2 (n=4 biological replicates, ANOVA $F_{2,11}$=4.934, p=0.0295; Tukey's *post hoc* multiple comparison test: *ROSA26* vs Δ*HS1332* *p < 0.05, *ROSA26* vs Δ*nMotif* *p<0.05); HNF3B (n=5 biological replicates, ANOVA $F_{3,16}$=5.297, p=0.0100; Tukey's *post hoc* multiple comparison test: *ROSA26* vs Δ*HS1332* **p<0.01, *ROSA26* vs Δ*nMotif* p<0.05); SMA (n=3 biological replicates, $F_{2,6}$=0.09587, p=0.9099; Tukey's *post hoc* multiple comparison test: *ROSA26* vs Δ*HS1332* p>0.05, *ROSA26* vs Δ*nMotif* p>0.05). ns, not significant.

(D) Single-cell RNA sequencing data from teratomas in UMAP representations. Clusters are labeled by cell identity (left). A comparison of *ROSA26* vs Δ*HS1332* (center) and *ROSA26* vs Δ*nMotif* (right) clusters with color coding is shown. Epi, epithelium; CycProg, cycling progenitors; Prog, progenitors; MSC, mesenchymal stem cells; Fib, fibroblasts; Myofib, myofibroblasts.

(E) Bar graph representing the proportion of cells sequenced in each condition falling into an ectodermal, endodermal, or mesodermal identity.

(F) scRNA-seq UMAP representation in which only ectodermal clusters from the prior UMAP (D) were extracted and re-clustered with identities assigned (left). Comparisons of ectodermal sub-clustering in *ROSA26* vs Δ*HS1332* (center) and *ROSA26* vs Δ*nMotif* (right) with color coding are shown.

Figure 4. Depletion of forebrain identity by excision of *HS1332*

(A) Gene Ontology (GO) terms depleted in ΔHS1332 and ΔnMotif vs ROSA26 teratomas in scRNA-seq analysis.

(B) Violin plots of expression of *FOXG1* (left) and *EMX2* (right) transcripts across ectodermal clusters in scRNA-seq datasets.

(C) Immunofluorescence microscopy of FACS-sorted GFP-positive rosettes stained for FOXG1, PLZF, and SOX2 in hESC derived rosettes. PLZF is a TF marker of rosette progenitors.[46,72]

(D) Graphical representation of cerebral organoid generation from hESCs.

(E) Organoids from the *ROSA26*, Δ*HS1332*, and Δ*nMotif* conditions at the 30 (left) and 40 (right)-day time-points were stained for the forebrain markers FOXG1 and EMX1, neuronal markers NeuN and TUJ1, SOX2 and GFP.

507 **Figure 5. Effects of *HS1332* excision and 3D chromatin loop perturbation on chromatin**
508 **modifications and 3D architecture in the *SOX2* TAD**
509 (A) Genome browser view of H3K27ac ChIP-sequencing in the *SOX2* TAD in hESCS using RPGC-
510 normalized signal track and rosettes using input-normalized ppois signal track.
511 (B) Genome browser view of RPGC-normalized H3K27me3 ChIP-sequencing in the *SOX2* TAD in
512 hESCS and rosettes. Additional data for peaks 1-3 are shown in Figure S6C.
513 (C) 4C-sequencing with a *SOX2* promoter bait in hESCS and rosettes.
514 (D) Significant interacting peaks, as determined by Benjamini-Hochberg multiple testing procedure
515 (red), in 4C-sequencing data of rosettes from the *ROSA26* and Δ*nMotif* conditions (*p<0.05).

516

517 **Figure 6. Loss of *SOX2* local chromatin organization affects *SOX2* expression and neuroglial**
518 **differentiation in mature NSCs**
519 (A) Agarose gel electrophoresis of PCR product containing the n*Motif* domain in control (NT-gRNA) vs
520 Δ*nMotif* NSCs (left). The Sanger sequencing results of the two PCR products is also shown (right).
521 (B) qRT-PCR for *SOX2* transcript in control and Δ*nMotif* NSCs (n=3 biological replicates, t-test
522 **p<0.01)
523 (C) Immunofluorescence microscopy for SOX2 and NESTIN in control vs Δ*nMotif* NSCs.
524 (D) Growth/viability measurement by WST8 absorbance assay in control and Δ*nMotif* NSCs (n=3
525 biological replicates, two-way ANOVA n=3, $F_{3,6}$=32.1 p<0.01; Sidak's multiple comparisons test
526 **p<0.01 at indicated timepoints).
527 (E) Immunofluorescence microscopy for TUJ1 and GFAP in neuronal and astrocytic differentiation of
528 control and ΔnMotif NSCs.
529 (F) qRT-PCR of neuronal transcript *RBFOX3* and astrocytic transcript *SLC1A2* after neuronal and
530 astrocytic differentiation of control and Δ*nMotif* NSCs (n=3 biological replicates, t-test p=0.0091 and
531 p=0.0171, respectively).
532 (G) Genome browser view of *SOX2* TAD comparing the following assays in NeuN+ or NeuN- cells
533 isolated from postmortem DLPFC in PsychEncode: ATAC-Sequencing, H3K27ac ChIP-
534 sequencing, *SOX2* promoter virtual 4C-sequencing, and *HS1332* enhancer virtual 4C-sequencing.
535 (H) HiC plots of the *SOX2* TAD in NeuN+ or NeuN- cells of postmortem DLPFC show preservation of
536 3D architecture in adult neurons and glia.

537
538

539 ## TABLES AND TEXT BOXES

540 **Table 1. gRNAs used for targeted CRISPR deletions**

gRNA ID	Sequence	Target
nMotif-grna1	GTCAGGACAAAGGACCATAG	nMotif
nMotif-grna2	TATTGGGTGTAACGTGGTTA	nMotif
HS1332-grna1	ATTTGCCCATCAATACACAG	HS1332
HS1332-grna2	CTATGTGGATAAAGTCCAGA	HS1332
Rosa26-gRNA	GCTAGCCTCTTGTCGCCGAT	ROSA26
NT-gRNA	GTATTACTGATATTGGTGGG	Non-targeting

541
542
543 **Table 2. Primers for Genotyping Deletions**

Genotyping Target	Sequence
nMotif	CTTCCCCAGGTTGCTCAATA
nMotif	GTACATGTCTGCATATCT
HS1332	ATCATTGCTGAGAAAAGGGT
HS1332	GATAGGGTTTGGTGACTTGCCAAGGTCA

544
545
546 **Table 3. 4C-Sequencing Primers: Sequences containing 4C bait sequences and sequencing**
547 **adapters**

Target	Sequence
SOX2 Promoter 5'	AATGATACGGCGACCACCGAGATCTACACTCTTTCCCTACACGACGCTCTTCCGATCTCGTGATTCCACTCTCTTGTTGGGATC
SOX2 Promoter 3'	CAAGCAGAAGACGGCATACGAGATAGGTCGCAGTGACTGGAGTTCAGACGTGTCTCTTCCGATCTCTTCTAGTCGGGACTGTGAG

548
549
550 **Table 4. Antibodies and Dilutions Used**

Manufacturer	Catalog #	Target	Immunofluorescence microscopy	Flow Cytometry
R&D Systems	AF2018	SOX2	1:100	
Abcam	Ab13970	GFP	1:500	
Biolegend	845502	TUJ1	1:500	
Agilent	Z033401	GFAP	1:500	
Neuromics	MO15012	Nestin	1:500	
Cell Signaling	60433S	PAX6	1:200	
Abclonal	A17910	SMA	1:200	
R&D systems	AF2400	HNF3β	1:200	
Santa Cruz	Sc-22839	PLZF	1:100	
Abcam	Ab18259	FOXG1	1:200	
Thermo Fisher	PA5-35373	EMX1	1:200	
Thermo Fisher	MA5-33103	NeuN	1:200	
Santa Cruz	Sc-5279	Oct3/4	1:100	

Miltenyi	REA101	SSEA4		1:100
Miltenyi	REA246	TRA-1-81		1:100

551
552
553
554

555 **STAR★METHODS**

556 **KEY RESOURCES TABLE**

Reagent or Resource	Source	Catalog number	RRID
Antibodies			
SOX2	R&D Systems	AF2018	AB_355110
GFP	Abcam	Ab13970	AB_300798
TUJ1	BioLegend	845502	AB_2566589
GFAP	Agilent	Z033401	AB_10013382
NESTIN	Neuromics	MO15012	AB_2148919
PAX6	Cell Signaling Technology	60433	AB_2797599
SMA	ABclonal	A17910	AB_2861755
HNF3β	R&D Systems	AF2400	AB_2294104
PLZF	Santa Cruz	Sc-22839	AB_2304760
FOXG1	Abcam	Ab18259	AB_732415
EMX1	Thermo Fisher	PA5-35373	AB_2552683
NeuN	Thermo Fisher	MA5-33103	AB_2802653
OCT3/4	Santa Cruz	Sc-5279	AB_628051
NANOG	Novus	NBP1-47427SS	AB_10010380
SSEA4	Miltenyi	130-115-875	AB_2653521
TRA-1-81	Miltenyi	130-123-334	AB_2802023
REA Control Antibody (S), human IgG1	Miltenyi	130-113-444	AB_2734114
Goat anti-Chicken IgY (H+L), Alexa Fluor 488	Life Technologies	A-11039	AB_2534096
Donkey anti-Goat IgG (H+L), Alexa Fluor 647	Life Technologies	A32849	AB_2762840
Donkey anti-goat IgG Alexa Fluor 555	Life Technologies	A21432	AB_2535853
Donkey anti-Rabbit IgG (H+L), Alexa Fluor Plus 488	Life Technologies	A32790	AB_2762833
Donkey anti-Rabbit IgG (H+L), Alexa Fluor Plus 555	Life Technologies	A32794	AB_2762834
Donkey anti-Mouse AlexaPlus 488 IgG (H+L)	Life Technologies	A32766	AB_2762823
Donkey anti-Mouse AlexaPlus 555 IgG (H+L)	Life Technologies	A32773	AB_2762848
ChIP-seq Antibodies and Key Reagents			
Tri-Methyl-Histone H3 (Lys27) (C36B11) Rabbit mAB	Cell Signaling Technology	9733	AB_2616029
Rabbit polyclonal Histone H3 (acetyl K27)	Abcam	Ab4729	AB_2118291
CTCF (D31H2) Rabbit mAB	Cell Signaling Technology	3418	AB_2086791
Rabbit IgG Isotype Control	Diagenode	C15410206	AB_2722554
Dynabeads Protein A	Invitrogen	10001D	

Sequencing Library Preparation Reagents			
Roche Expand Long Template PCR (4C Library Preparation)	Roche	11681834001	
NEBNext High-Fidelity 2X PCR Master Mix (ChIP-seq and ATAC library preparation)	NEB	M0541L	
Monarch Spin RNA Isolation Mini Kit	NEB	T2110S	
AMPure XP Beads	Beckman Coulter	A63880	
Phenol:Chloroform:Isoamyl Alcohol 25:24:1 Saturated with 10 mM Tris, pH 8.0, 1 mM EDTA (4C)	Sigma	P2069	
Glycogen (4C)	Invitrogen	10814010	
RNAse A (4C)	Thermo	EN0531	
Proteinase K	NEB	P8107S	
Single Cell Multiome ATAC+Gene expression	10X genomics	1000283	
Arima HiC+ Library Preparation Kit	Arima Genomics	A510008	
KAPA Hyperprep Kit	Roche	07962347001	
20% Methanol	Tousimis Research	1008A	
Digitonin	Promega	G9441	
T4 DNA Ligase	NEB	M0202T	
2X TD buffer	Illumina	20034198	
Illumina Tagment DNA Enzyme	Illumina	20034198	
MinElute Reaction Cleanup Kit	Qiagen	28204	
Agilent High Sensitivity D1000 ScreenTape	Agilent	5067-5584	
High Sensitivity ScreenTape Reagents	Agilent	5067-5585	
KAPA Library Quantification	Roche	07960140001	
Qubit™ dsDNA High-Sensitivity	Life Technologies	Q33230	
DNA FISH Reagents			
KAPA HiFi HotStart ReadyMix	Roche	50-196-5217	
QIAquick PCR Purification Kit	Qiagen	28104	
HiScribe T7 High Yield RNA Synthesis Kit	NEB	E2040S	
NucleoSpin RNA Clean-up Kit	Macherey-Nagel	740948.50	
SuperScript IV Reverse Transcriptase	Thermo Fisher	18090010	
dNTPs	NEB	N0447S	

Exonuclease I	NEB	M0293S	
the Zymo Quick-RNA Miniprep Kit	Zymo Research	R1054	
RNase H	NEB	M0297S	
RNase A	Thermo Scientific	EN0531	
Cy5	Cytiva	PA15101	
FISH Tag DNA Kits	Thermo Fisher	F32948	
Microscopy Key Reagents			
FocusClear	CelExplorer	FC-101	
Western Blot Reagents			
RIPA Buffer	Thermo Fisher	89900	
Halt Protease Inhibitor	Thermo Fisher	78429	
Bioruptor	Diagenode	UCD-300	
DC protein assay kit	Bio-Rad	5000112	
Laemmli buffer	Bio-Rad	1610747	
0.2 µm nitrocellulose membranes	Bio-Rad	1620112	
Plasmids			
pMD2.G (lentiviral packaging plasmid)	Addgene	12259	Addgene_12259
psPAX2	Addgene	12260	Addgene_12260
LentiCRISPRv2-mCherry	Addgene	99154	Addgene_99154
pDonor_mU6	Addgene	69350	Addgene_69350
LentiCRISPRv2GFP	Addgene	82416	Addgene_82416
Taqman qPCR Probes			
RBFOX3	Invitrogen	Hs01355808	
TUBB3	Invitrogen	Hs00801390_s1	
SLC1A2	Invitrogen	Hs01102423	
SOX2	Invitrogen	Hs01053049_s1	
GAPDH	Invitrogen	Hs02758991_g1	
FOXG1	Invitrogen	Hs01850784_s1	
Chemicals, peptides, and recombinant proteins			
FGF8a recombinant protein	R&D Systems	4745-F8	
SHH recombinant protein	PeproTech	100-45-25ug	
FGF2 recombinant protein	R&D Systems	4114TC	
EGF recombinant protein	R&D Systems	236EG	
SB431542	MedChemExpress	HY-10431	
LDN193189	Thermo Fisher	605310	
Y-27632 ROCK inhibitor	MedChemExpress	HY-10071	
BDNF	R&D Systems	248-BDB-050	
Ascorbic Acid	Sigma	A4403-100mg	
Cell Lines			

H9 *Hes5::GFP* hESC	Placantonakis Lab		
HEK293T	Clontech Takara	632180	CVCL_4401
H9 Neural Stem Cells	Placantonakis Lab		
Mouse embryonic Fibroblasts (mitomycin treated)	Thermo Fisher	A34958	CVCL_RB06
Software			
ImageJ	https://imagej.net/		SCR_003070
Rstudio	The R Foundation		SCR_000432
Seurat	Rahul Satija Lab		SCR_016341
Integrated Genomics Viewer (IGV)	Broad Institute		SCR_011793
GraphPad Prism 10	www.graphpad.com		SCR_002798
Trimmomatic	https://github.com/timflutre/trimmomatic		SCR_011848
Trim Galore	https://github.com/FelixKrueger/TrimGalore		SCR_011847
Bowtie 2	https://github.com/BenLangmead/bowtie2/releases		SCR_016368
Samtools	https://www.htslib.org/		SCR_002105
Deeptools	https://github.com/deeptools/deepTools		SCR_016366
HOMER	http://homer.ucsd.edu/homer/		SCR_010881
HiC Bench	https://github.com/NYU-BFX/hic-bench		
4Cker	https://github.com/rr1859/R.4Cker		
DeSeq2	https://bioconductor.org/packages/release/bioc/html/DESeq2.html		SCR_015687
FlowJo	https://www.flowjo.com/solutions/flowjo		SCR_008520
ShinyGO	http://bioinformatics.sdstate.edu/go/		SCR_019213
Seq-n-Slide (sns)	https://igordot.github.io/sns/		
UCSC Genome Browser	http://genome.ucsc.edu/		SCR_005780
Deposited Data			
HiC in NSCs	This study	GEO PENDING	
H3K27ac ChIP in NSCs	This study	GEO PENDING	
H3K27me3 ChIP in NSCs	This study	GEO PENDING	
CTCF ChIP in NSCs	This study	GEO PENDING	
H3K27ac ChIP in rosette NSCs	This study	GEO PENDING	
H3K27me3 ChIP in rosette NSCs	This study	GEO PENDING	
4C-sequencing in rosette NSCs	This study	GEO PENDING	
scRNA-seq in teratomas	This study	GEO PENDING	

4C-sequencing in hESCs	This study	GEO PENDING	
H3K27ac ChIP in hESCs	This study	GEO PENDING	
H3K27ac ChIP in hESCs	This study	GEO PENDING	
4C-sequencing in hESCs	This study	GEO PENDING	
Public datasets reanalyzed			
HiC in hESCs	Dixon et al. [73]	GSE52457	
CTCF ChIP in hESCs	ENCODE	ENCSR871MKQ	
HiC in mESCs	Bonev et al. [74]	GSE96107	
H3K27ac ChIP in mESCs	ENCODE	ENCSR000CGQ	
H3K27me3 ChIP in mESCs	ENCODE	ENCSR059MBO	
CTCF ChIP in mESCs	Bonev *et al.* [74]	GSE96107	
HiC in mNSCs	Bonev *et al.* [74]	GSE96107	
H3K27ac ChIP in mNSCS	Bonev *et al.* [74]	GSE96107	
H3K27me3 ChIP in mNSCs	Bonev *et al.* [74]	GSE96107	
CTCF ChIP in mNSCs	Bonev *et al.* [74]	GSE96107	
hESC-Mesoderm HiC	Zhang *et al.* [40]	GSE186958	
hESC-Mesoderm H3K27ac ChIP	Zhang *et al.* [40]	GSE186958	
hESC-Mesoderm H3K27me3 ChIP	Zhang *et al.* [40]	GSE186958	
hESC-Mesoderm RNAseq	Zhang *et al.* [40]	GSE186958	
Zebrafish HiC Brain	Yang et al. [75]	GSE134055	
Zebrafish HiC Muscle	Yang *et al.* [75]	GSE134055	
Zebrafish H3K27ac ChIP Brain	Yang *et al.* [75]	GSE134055	
Zebrafish H3K27me3 ChIP Muscle	Yang *et al.* [75]	GSE134055	
DLPFC HiC	PsychENCODE[76]	syn21760712	
DLPFC H3K27ac ChIP	PsychENCODE	syn4566010	
DLPFC ATAC-seq	PsychENCODE	GSE83345	
Culture Media, Media Components, and Culture reagents			
DPBS	Gibco	14190-144	
DMEM/F12	Gibco	11330032	
DMEM, high glucose	Gibco	11965-118	
Pluristem ESC/iPSC Feeder Free Media	Sigma	SCM130	
Knockout Serum Replacement	Thermo Fisher	10828028	
Fetal Bovine Serum	Peak Serum	PS-FB2	
N2 Media Supplement	Thermo Fisher	17-502-049	
B27 Media Supplement	Thermo Fisher	12587010	
Insulin from Bovine Pancreas	Sigma	I0516	

Glucose for Cell Culture (1.6g/L)	Fisher	A2494001	
STEMdiff Cerebral Organoid Kit	Stemcell Technologies	8570	
OptiMEM	Gibco	31985062	
APEL2 Medium	Stemcell technologies	5270	
Dispase	Sigma	SCM133	
Trypsin-EDTA 0.5%	Fisher	25300054	
TrypLE Express Enzyme (1X)	Gibco	12604013	
Defined Trypsin Inhibitor	Fisher	A2494001	
Lenti-X Concentrator	Takara	631231	
Laminin	Fisher	23017015	
Poly-L-Ornithine 0.1%	R&D Systems	3436-100-01	
Matrigel	Corning	354277	
Geltrex	Thermo Fisher	A1569601	
Accutase	Thermo Fisher	A1110501	

557
558

559 ## EXPERIMENTAL MODEL AND STUDY PARTICIPANT DETAILS

560 ### H9 hESC culture

561 H9 (WA09) human embryonic stem cells (hESCs) stably nucleofected with a *Hes5::GFP* reporter were
562 cultured as colonies on a layer of mouse embryonic fibroblasts (MEFs, Invitrogen) in hESC medium,
563 consisting of 1:1 DMEM/F12 (Invitrogen), 20% KSR (Invitrogen), 5 ng/mL FGF2 (R&D), 2 mM glutamine
564 (Invitrogen), 0.1 mM non-essential amino acids (Invitrogen), and 0.1 mM β-mercaptoethanol (Invitrogen).[43]
565 Cultures were routinely groomed of differentiating colonies and fed daily. Passaging was performed with
566 dispase (Invitrogen) or by mechanically picking colonies. Dissociation to single cells was performed with
567 Accutase (Thermo Fisher) and subsequent culture of cells in hESC medium supplemented with 10 μM Y-
568 27632 ROCK inhibitor (MedChemExpress) for the first 24 hours. All hESC experimentation was approved
569 by ESCRO (protocol #14-00267) at NYU Grossman School of Medicine. Cells were cultured in humidified
570 cell culture incubators at 37 °C with room air balanced with 5% CO_2.

571

572 ## METHOD DETAILS

573 ### HEK293T cell culture and lentivirus production

574 Human embryonic kidney 293 T cells (HEK293T, Takara, Cat# 632180) were cultured in Dulbecco's
575 Modified Eagle's Medium (DMEM, Gibco) supplemented with sodium pyruvate (Gibco) and 10% fetal
576 bovine serum (FBS; Peak Serum) at 37 °C and 5% CO_2 in humidified room air. HEK293T cells were co-
577 transfected with plasmid DNAs consisting of the lentiviral transfer vector, as well as the pMD2.G and
578 psPAX2 packaging plasmids using Lipofectamine 2000 (Invitrogen). Medium was harvested for 3
579 consecutive days with Lenti-X Concentrator (Takara) added at 1:4 and stored at 4 °C. Virus-containing
580 medium was centrifuged at 1500xg for 45 minutes at 4 °C to concentrate the viral particles. Viral particles
581 were resuspended in Opti-MEM (Thermo Fisher), aliquoted, and stored at -80 °C until use.
582

583 ### CRISPR genome editing

584 Flanking gRNAs for target motifs or enhancers were designed using Benchling with on-target and off-target
585 scores calculated according to published methods. Dual gRNA inserts were cloned into LentiCRISPRv2-
586 mCherry in accordance with previously published methods.[77,78] In short, oligos containing both gRNAs
587 (Table 1) were acquired from Eurofins Genomics and then PCR-amplified to create a fragment which was
588 subcloned into a *U6* promoter-containing donor construct. The resulting dual promoter and dual gRNA
589 fragment was cloned into one of the previously listed LentiCRISPRv2 constructs. Successful cloning was
590 confirmed by diagnostic digest with XhoI and NotI (New England Biolabs), followed by Sanger sequencing
591 of the gRNA insert. Lentivirus was generated in HEK293T cells by cotransfection with the packaging
592 plasmids pMD2.G and psPAX2 as previously described.[79] hESCs or NSCs were transduced with lentivirus
593 at a multiplicity of infection of 1. mCherry-positive hESCs were FACS-sorted in hESC medium
594 supplemented with 10 μM Y-27632 and expanded in MEF cultures. To obtain hESC clones with the desired
595 CRISPR modifications, we dissociated hESC colonies to single cells using Accutase (Thermo Fisher) and
596 the resulting suspension was filtered through a 40 μm filter to ensure a single cell suspension. Individual
597 cells were seeded on MEFs in 24 well tissue culture plates at 1,2,4 and 5 cells per well. Only the 5 cell/well
598 condition produced colonies at a rate of 1 for every 24 wells seeded. mCherry-positive NSCs were FACS-
599 isolated and pooled cell cultures were grown for two weeks before genotyping.
600

601 ### Genotyping of modified cell lines

602 Human ESCs and NSCs selected for expression of lentiCRISPR dual gRNA constructs were genotyped
603 using primers flanking the modified loci (Table 2). Resulting PCR products were run on 1% agarose gels
604 containing SYBR Safe (Thermo) for visualization and imaged using an Invitrogen iBright. PCR products in
605 modified cell lines were extracted from agarose gels and Sanger-sequenced to verify deletion at the
606 predicted motifs. Human ESC clones and NSCs with verified deletions were then used for all subsequent
607 analyses.
608

609 ### Directed hESC to rosette-NSC differentiation *in vitro*

610 Human ESC to rosette-NSC (rosette) differentiation was performed, as previously described.[54] Briefly,
611 hESCs were plated on Geltrex-coated plates at ~50,000 cells/cm^2 and grown under feeder-free conditions

612 in Pluristem Human ES Cell Medium (Millipore) until reaching ~80% confluence. Medium was then changed
613 first to KSR medium [Knockout-DMEM, 15% knockout serum replacement (KSR), 2 mM L-glutamine, 1X
614 nonessential amino acids (NEAA), and 0.1% β-mercaptoethanol] supplemented with 10 μM SB-431542
615 (stemMACS) and 100 nM LDN-193189 (Fisher) to achieve dual SMAD inhibition. KSR concentration was
616 gradually reduced over 10 days in exchange for N2 medium: on day 2, medium was changed to 75% KSR
617 medium + 25% N2 Medium [1:1 DMEM/F12 (Invitrogen), N2 supplement 1X, and 1.6 g/L glucose], again
618 supplemented with SB-431542 and LDN-193189; on days 4, 6, and 8, medium was changed with a 25%
619 decrease in KSR medium composition every two days, until on day 8 the medium consisted of 100% N2
620 with SB-431542 and LDN-193189.
621
622 **NSC culture and differentiation**
623 Human ESC-derived NSCs were cultured in DMEM/F12 medium (Thermo) supplemented with N2
624 supplement 1X (Fisher), B27 supplement 0.1X (Fisher), insulin (Sigma), glucose (1.6 g/L) (Fisher), 20
625 ng/mL EGF (R&D Systems) and 20 ng/mL FGF2 (R&D Systems). Cells were cultured on plates coated for
626 24 hours with 0.025% poly-L-ornithine (Gibco) followed by 2 hours of coating with 10 μg/mL of laminin in
627 PBS (Gibco). Medium was changed every 48 hours. Cells were passaged upon reaching confluence with
628 Trypsin (Invitrogen) and Defined Trypsin Inhibitor (Invitrogen) onto freshly coated plates at a 1:2 passaging
629 dilution. Low-passage cell cultures were used for all experiments.
630
631 **Neuroglial differentiation**
632 For neuronal differentiation, rosettes or NSCs maintained in EGF/FGF2 were cultured in N2 medium with
633 20 ng/mL BDNF (R&D) and 200 nM Ascorbic Acid (Sigma). Medium and growth factors were replaced
634 every two days for 30 days before analysis. Astrocytic differentiation was performed with 4% FBS
635 (Invitrogen) in N2, with fresh medium changed every two days for 42 days. Cells were cultured in humidified
636 cell culture incubators at 37 °C balanced with 5% CO_2. Biological replicates represent differentiations
637 performed on different days using newly seeded rosettes or NSCs maintained in EGF/FGF2.
638
639 **Serum-free embryoid body (SFEB) culture**
640 Mature hESC colonies grown on MEF plates were dissociated using dispase (Sigma). The resulting
641 colonies were collected, resuspended in APEL2 serum-free media (Stemcell Technologies), and triturated
642 by pipetting 3 times to break up mature colonies into smaller colonies. Around 15-20 colonies were plated
643 on low-attachment 24-well plates (Thermo Fisher) in 500 ml of APEL2 medium.[45] Medium was refreshed
644 every 5 days with new APEL2 medium and SFEBs were monitored by wide-field microscopy to assess GFP
645 fluorescence.
646
647 **hESC teratoma formation assay**
648 Male NSG mice at 6 to 8 weeks of age were anesthetized using an anesthetic of ketamine and xylazine
649 diluted in PBS at 100 mg/kg and 20 mg/kg, respectively. After induction of anesthesia, each flank was
650 sterilized with 70% ethanol and shaved. Subsequently, $1x10^6$ dissociated hESCs in 50 mL of a 1:1 mixture
651 of DMEM/F12 (Invitrogen) and Matrigel (Corning) was drawn into a 17-gauge needle and injected into the
652 flank. Teratomas were allowed to grow for 6 weeks. Teratoma tissue was harvested following euthanasia
653 through injection with 50 mg/kg of pentobarbitol (Euthasol, Virbac). Procedures were performed according
654 to IACUC protocol number 160403 at NYU Grossman School of Medicine.
655
656 **Cerebral organoid culture**
657 Cerebral organoids were made using the forebrain cerebral organoid kit from StemCell Technologies. To
658 generate the initial embryoid bodies, low-passage hESC colonies were dissociated to single cells using
659 Gentle Dissociation Reagent and resuspended in Basal Medium 1 with Supplement A containing 10 μM Y-
660 27632 at a concentration of 150,000 cells/mL. One hundred μL of the cell suspension was plated in ultra-
661 low attachment round-bottom 96-well plates (Corning) and incubated for five days, with fresh medium added
662 every other day. At the 5-day mark, embryoid bodies were transferred to low-attachment 24-well plates and
663 grown for 2 days in induction media composed of Basal Medium 1 and supplement B. At day 7, embryoid
664 bodies were embedded in Matrigel on a sterile embedding surface, transferred into low-attachment 6-well
665 plates, and maintained in expansion media for 3 days. Beginning on day 10 and continuing through day 30
666 or 40, cerebral organoids were maintained in maturation media, which was changed every 3 days until
667 organoids were harvested.

668
669 **Chromatin immunoprecipitation (ChIP) sequencing**
670 ChIP-Sequencing libraries were prepared according to the ChIPmentation protocol previously published.[80]
671 In short, hESCs or their rosette progeny were fixed in 1% paraformaldehyde (PFA) for 10 minutes at room
672 temperature (RT) and quenched with a final concentration of 0.125 M glycine for 5 minutes. Fixed cells
673 were lysed and sonicated using a Diagenode Bioruptor for 15 cycles at 30 seconds on, 30 seconds off on
674 the "high" sonication setting. Proper chromatin shearing with the desired fragment length in the 200-600 bp
675 range was confirmed by agarose gel electrophoresis. Chromatin was incubated at 4 °C overnight with
676 antibody-conjugated dynabeads. Beads were washed and chromatin was tagmented using Tn5
677 transposase (Illumina). DNA was de-crosslinked by proteinase K digestion and was purified using the
678 Qiagen MinElute kit. Tagmented, de-crosslinked DNA was PCR-amplified using single barcoded primers
679 and was sequenced with a target sequencing depth of >30 M reads for H3K27ac or CTCF ChIP, and >50M
680 reads for H3K27me3 ChIP samples.
681
682 **Assay for Transposase-Accessible Chromatin (ATAC) sequencing**
683 We used an improved ATAC-seq protocol (Omni-ATAC) adopted from Corces et al.,[81] with small
684 adaptations. After counting, 100,000 cells were collected, resuspended in 1X cold DPBS (Gibco) and
685 centrifuged at 500xg for 5 min at 4 °C. After centrifugation, the supernatant was removed and the cell pellet
686 resuspended in 500 μL of cold ATAC-seq resuspension buffer 1 (10 mM Tris-HCl pH 7.4, 10 mM NaCl, 3
687 mM $MgCl_2$, 0.1% NP-40 and 0.1% Tween-20 in H_20). Fifty μL (50,000 cells) were transferred to a new
688 1.5 ml Eppendorf tube and 0.5 μL 1% Digitonin (Promega) was added by pipetting well a few times. The
689 cell lysis reaction was incubated on ice for 3 min. After lysis, 1 mL of cold ATAC-seq resuspension buffer 2
690 (10 mM Tris-HCl pH 7.4, 10 mM NaCl, 3 mM $MgCl_2$ and 0.1% Tween-20 in H_20) was added. The tube was
691 inverted three times to mix the contents and nuclei were pelleted by centrifugation for 10 min at 500xg at 4
692 °C. The supernatant was carefully removed and nuclei were resuspended in 45 μL of transposition mix
693 [25 μL 2X TD buffer (Illumina), 16.5 μL 1X PBS, 0.5 μL 1% digitonin, 0.5 μL 10% Tween-20 and 2.5 μL
694 H_2O) by pipetting up and down a few times. Five μL of transposase enzyme (Illumina) was then added and
695 the transposition reaction was incubated at 37 °C for 30 min in a thermomixer with shaking at 1000 rpm.
696 The reaction was cleaned up with MinElute Reaction Cleanup Kit (Qiagen). Transposed DNA fragments
697 were then amplified as described previously in Buenrostro et al.[82] Final libraries were purified with Ampure
698 XP Beads (Beckman), checked by Tapestation High Sensitivity (Agilent) and quantified by Qubit (Life
699 Technologies). Libraries were then sequenced with the Novaseq6000 Illumina Sequencing System with
700 150 bp paired-end reads.
701
702 **RNA Sequencing**
703 RNA was extracted from $5x10^6$ freshly harvested hESCs or NSCs using the Monarch Spin RNA Isolation
704 Mini Kit (NEB). Quality was verified by an Agilent Bioanalyzer 2100. RNA-seq libraries were generated by
705 the NYU Genome Technology Center using the Illumina Ribo-Zero Plus rRNA Depletion Kit and sequenced
706 on the Illumina NovaSeq X with 50 bp paired-end reads. RNA-seq fastq files were processed in route "rna-
707 star" using the Seq-n-Slide (sns) pipeline: https://igordot.github.io/sns/. Alignment of reads was performed
708 using the hg19 assembly of the human genome. BAM alignment files were processed to BigWig using
709 deeptools and visualized using the UCSC genome browser.[83,84]
710
711 **HiC library preparation**
712 Human ESCs or NSCs were dissociated and counted, and $1x10^6$ cells were crosslinked with 2% methanol-
713 free formaldehyde (Tousimis) in PBS for 10 minutes at RT. The reaction was quenched with glycine to a
714 final concentration of 0.125 M. The cell suspension was then centrifuged and the supernatant was removed.
715 Cells were washed twice with PBS and processed using the HiC+ kit from Arima Genomics. In short,
716 crosslinked cells were incubated with multiple restriction enzymes to digest chromatin. Arima-HiC
717 sequencing libraries were prepared by first shearing purified proximally ligated DNA and then size-selecting
718 200-600 bp DNA fragments using SPRI (Solid Phase Reversible Immobilization) beads. The size-selected
719 fragments were then enriched using Enrichment Beads (provided in Arima HiC kit), and then converted into
720 Illumina-compatible sequencing libraries with TruSeq adapters using the KAPA HyperPrep kit (Roche). The
721 purified, PCR-amplified libraries underwent standard quality control using KAPA qPCR and Tapestation

722 (Agilent) and were sequenced on the NovaSeq6000 Illumina Sequencing System with 150 bp paired-end
723 reads.
724
725 **4C library preparation**
726 Cells were processed for 4C-Seq as previously described.[38] Cells were dissociated and counted, and $1x10^7$
727 cells were crosslinked with 2% methanol-free formaldehyde (Tousimis) in PBS for 10 minutes at RT. The
728 reaction was quenched with glycine to a final concentration of 0.125 M. After centrifugation, the cell pellet
729 was resuspended in 1 mL of lysis buffer (50 mM Tris, 150 mM NaCl, 5 mM EDTA, 0.5% NP-40, 1% Triton
730 X-100 and 1X Roche complete protease inhibitor). Cells were incubated on ice for 15 minutes and then
731 centrifuged at 2500 RPM at 4 °C for 5 minutes. Pellets were resuspended in 360 μL of molecular grade
732 H_2O, 60 μL of DpnII restriction buffer and 15 μL of 10% SDS. Samples were incubated at 37 °C for 1 hour
733 shaking at 900 RPM. One hundred fifty μL of 10% Triton X-100 was added and samples were further
734 incubated at 37 °C for 1 hour at 900 RPM. A 5 μL sample was taken and stored for comparison with the
735 prepared template. Nuclei were incubated overnight with 200 units of DpnII (New England Biolabs)
736 restriction enzyme. Eighty μL of 10% SDS were added and samples were then incubated at 65 °C for 30
737 minutes to inactivate the DpnII enzyme. Samples were brought up to 7 mL and proximity-ligated using 4000
738 units of T4 DNA ligase (NEB) overnight at 16 °C. Crosslinks were reversed by addition of 30 μL of proteinase
739 K and incubation overnight at 65 °C with shaking. Thirty μL of RNase A were then added and samples were
740 incubated at 37 °C to eliminate RNA. Samples were phenol/chloroform/isoamyl alcohol (Sigma)-extracted
741 and DNA was ethanol precipitated. A subsequent restriction digestion was performed in 500 μL total volume
742 using 50 units of Csp6I (Fermentas). Samples were incubated at 65 °C for 30 minutes to inactivate the
743 enzyme and another proximity ligation reaction was performed in 14 mL total volume using 6000 units of
744 T4 DNA ligase (NEB). DNA was again phenol/chloroform-extracted and ethanol precipitated. DNA was
745 resuspended in 10 mM Tris pH 8.0 and purified using QIAquick PCR purification kits. DNA was quantified
746 by Qubit fluorometry.
747 DpnII/Csp6I 4C templates were PCR-amplified using Expand Long Template PCR System (Roche). In brief,
748 400 ng of template was used as input in 50 μL PCR reactions using single barcode primers containing the
749 *SOX2* promoter bait, as listed in Table 3. Libraries were isolated using QIAquick PCR purification (Qiagen)
750 and quantified by Qubit and KAPA qPCR (Roche) prior to sequencing.
751
752 **Preparation of single cell RNA sequencing libraries from teratoma tissues**
753 Previously harvested, flash-frozen teratoma tissue samples were lysed by addition of 0.1 mL of freshly
754 prepared 0.1X lysis buffer (10 mM Tris-HCl, 10 mM NaCl, 3 mM $MgCl_2$, 0.1% Tween-20, 0.1% NP40, 0.01%
755 digitonin, 1% BSA, 1 mM DTT, and 1 U/mL Sigma protector RNase inhibitor), tissue homogenized with
756 microfuge tube pestles, and incubated on ice for 10 minutes. One mL of chilled wash buffer (10 mM Tris-
757 HCl pH 7.4, 10 mM NaCl, 3 mM $MgCl_2$, 1% BSA, 0.1% Tween-20, 1 mM DTT, and 1 U/mL of RNase
758 inhibitor) was added and the mixture was strained through 70 and 40 µm filters. The resulting solution of
759 nuclei and debris was stained with 5-AAD and the mixture sorted for 5-AAD-positive nuclei on a FACSAria
760 cell sorter. Resulting nuclei were immediately processed to generate single cell RNA-sequencing libraries
761 using the 10X Genomics protocols in the Single Cell 3' Reagent Kits v2 User Guide. Data were processed,
762 normalized, integrated for all specimens, and clustered together using Seurat packages based on RNA.
763 Only cells with greater than 750 features and fewer than 0.10% mitochondrial genes were included in the
764 analysis. Initial labeling of all cells was performed using the reference mapping feature of Seurat against
765 data from McDonald and colleagues.[48,85]
766
767 **Next-generation sequencing**
768 Libraries made according to preceding ChIP, 4C, and HiC library protocols were quantified by Qubit
769 (Thermo Fisher) or KAPA qRT-PCR (Roche) and library quality assessed by Tapestation High Sensitivity
770 (Agilent) electrophoresis. Libraries were pooled as appropriate and sequenced on Illumina Novaseq6000
771 to achieve the targeted sequencing depth of ~50 M reads per sample for H3K27me3, ~30 M reads for
772 H3K27ac, ~25 M for ATAC-Seq, ~30 M for RNA-sequencing, ~5 M reads for 4C libraries, and ~500 M reads
773 for HiC libraries.
774
775 **Processing of sequencing datasets**

ChIP-Sequencing and ATAC-sequencing demultiplexed fastq files were trimmed using Trimmomatic, aligned against the Hg19 genome assembly using Bowtie2, and processed to BigWigs and Bed files for visualization using Samtools and Deeptools. Reads Per Genomic Content (RPGC)-normalized files were visualized using the UCSC genome browser or IGV (hg19 chr3:181000000-182500000) with the exception of H3K27ac in rosette NSCs, which was processed using MACS2 to produce Poisson p-value adjusted BigWigs.[84,86] Peak calling and differential peak analysis was performed using MACS2. HiC datasets were processed using the HiC-bench suite.[87] 4C-sequencing was mapped against a fragment library of the DpnII-Csp6I digested genome using 4Cker.[88]

qRT-PCR

Quantitative Real Time PCR for gene expression profiling was performed with the Cells-to-Ct kit (Invitrogen), Taqman Gene Expression kit (Invitrogen) and the StepOne Real Time PCR System (Invitrogen) as recommended by the manufacturers. Following the completion of the qPCR, extracted Ct values from the StepOne Software (v2.1) was then assessed to calculate the normalized target gene expression level using the ΔΔCt method to determine relative fold-change. The following TaqMan (Invitrogen) primers/probes were used: *RBFOX3* (Hs01355808), *TUBB3* (Hs00801390_s1), *SLC1A2* (Hs01102423), *SOX2* (Hs01053049_s1), *GAPDH* (Hs02758991_g1), *FOXG1* (Hs01850784_s1).

FISH (fluorescent *in situ* hybridization) probe synthesis

Oligo probes targeting the *HS1332* and anchor regions within the *SOX2* TAD were designed using paintSHOP[89] and ordered from IDT as oPools (probe sequences are listed in Supplementary Table 1). Single-stranded DNA (ssDNA) probe pools were diluted to 0.07 ng/μL and amplified using KAPA HiFi HotStart ReadyMix (Roche) with 100 μM forward and reverse primers specific to each probe set. PCR was performed with the following conditions: 95 °C for 3 min; 20 cycles of 98 °C for 20 s, 56 °C for 15 s, and 72 °C for 30 s; then 72 °C for 30 s. Debubbling mix was then added and the same PCR program was repeated twice. PCR products were purified using the QIAquick PCR Purification Kit (Qiagen). Purified double-stranded DNA templates (≥ 1 μg) were transcribed using the HiScribe T7 High Yield RNA Synthesis Kit (NEB) at 37 °C for 4–16 h. RNA was purified using the NucleoSpin RNA Clean-up Kit (Macherey-Nagel). Complementary DNA (cDNA) was then synthesized using SuperScript IV Reverse Transcriptase (Thermo Fisher) with 52 μg RNA template, 1 mM directly conjugated, fluorescently labeled RT primer, and 10 mM dNTPs (NEB, Cat. No. N0447S). Probes targeting *HS1332* received RT primers labeled with Cy5 (Cytiva), while those targeting the anchor control region used those labeled with Alexa fluor 555 (Thermo). Reactions were incubated at 50 °C for 4 h. Unincorporated primers were digested with Exonuclease I (NEB) at 37 °C for 15 min, followed by heat inactivation in 0.5 M EDTA, pH 8.0, at 80 °C for 20 min to generate RNA:DNA hybrids. RNA:DNA hybrids were purified using the Zymo Quick-RNA Miniprep Kit (Zymo Research, Cat. No. R1054). Residual RNA was digested using RNase H (NEB) and RNase A (Thermo Scientific) sequentially (37 °C for 2 h; 70 °C for 20 min; 50 °C for 60 min). The resulting single-stranded DNA (ssDNA) probes were purified using the Zymo Quick-RNA Miniprep Kit and eluted in 100 μL nuclease-free H_20.
The FISH probe library targeting a control locus (chr11, *HBB* locus) was ordered from Arbor Biosciences.

FISH sample staining

We performed DNA FISH based on previously published protocols with some modifications.[90-92] All steps were performed at RT unless otherwise specified. Samples were prepared on 1.5H coverslips, fixed in 4% PFA/PBS, rinsed three times in PBS and processed on the same day in 6-well plates. They were then permeabilized with 0.5% Triton X-100 in PBS for 10 min and rinsed for 3 min with PBS twice. Cells were incubated for 5 min in 0.1 N HCL, and rinsed three times for 1 min in 2XSSC (saline sodium citrate), then three times for 3 min in PBS. Cells were incubated in RNAse A at 37 °C for 1 h in a humid environment. Samples were pre-hybridized in preheated Hybridization #1 buffer [0.1% (v/v) Tween-20, 50% (v/v) formamide, 2XSSC] at 37 °C for 30 min in a humid environment. Meanwhile, the probe mix was prepared by complementing 2 pmol of each probe set with Hybridization #2 buffer [0.1% (v/v) Tween-20, 50% (v/v) formamide, 10% (v/v) dextran sulfate, 2XSSC] up to a 10 mL volume. The probe mix was then denatured for 5 min at 85 °C in the dark and chilled for 5 min on ice. Twenty mL of probe mix were added to each coverslip, which was then sealed onto a microscope slide with rubber cement in dark for 5 mins.
Sample chromatin was denatured by placing the slides for 5 mins at 85°C on an inverted heat block submerged in an 85 °C water bath. Slides were then transferred to a humidified slide tray and incubated overnight in the dark at 42 °C. The next day, the rubber cement was peeled off and the coverslip floated off

the slides in a 2XSSC reservoir. Coverslips were then transferred to 6-well plates pre-filled with probe wash buffer [0.1% (v/v) Tween-20, 50% (v/v) formamide, 5XSSC] and were incubated at 42 °C for 50 min in a humidified environment. This step was repeated with fresh probe wash buffer, then twice for 5 min in 5XSSCT (5XSSC with 0.1% Tween-20), and 5 min in PBS. Cells were stained with 4′,6-diamidino-2-phenylindole (DAPI) for 5 min and rinsed in PBS. Coverslips were mounted on Prolong Gold, allowed to cure for 24 h in the dark, sealed with nail polish, and imaged.

FISH sample imaging and analysis

FISH imaging was performed on a Nikon Eclipse Ti-2 inverted epifluorescence microscope controlled by MicroManager,[93] equipped with a Prime BSI Express camera, using a 100x oil-immersion lens (NA=1.4). Image stacks were captured with voxel size 64.5 x 64.5 x 250 nm. Slides were imaged using four channels: 405 nm (DAPI), 488 nm (chr11 control probe targeting the *HBB* locus), 532 nm (Alexa Fluor 555; chr3 anchor), and 637 nm (Cy5; *HS1332* sequence) excitation lasers.
Nuclei were segmented in 2D from maximum intensity projections of the DAPI signal using Cellpose.[94] FISH spots were detected in each channel using AIRLOCALIZE,[95] and the FISH spots were individually mapped to their matching nuclei based on their x,y coordinates using a custom MATLAB script.

Flow cytometry

Human ESC colonies were dissociated using TrypLE (Gibco**)** and $1x10^6$ cells were centrifuged at 300xg for 5 min before being washed with Dulbecco's phosphate buffered saline (Gibco). Cell pellets were then resuspended in fluorescence activated cell sorting (FACS) buffer (0.5% BSA in DPBS with 2 mM EDTA). Each sample was incubated with 2 μL of SSEA4 488 (Miltenyi), TRA-1-81 PE (Miltenyi) or an IgG1 isotype control antibody with matching fluorophore (Miltenyi) at 4 °C for 10 min. Cells were pelleted at 300xg for 5 min and washed twice with FACS buffer, before being resuspended in buffer with 100 ng DAPI for dead cell exclusion. Samples were analyzed by flow cytometry (BD LSRFortessa II – BD Biosciences) and resulting data was analyzed using FlowJo™ v10.8 Software (BD Life Sciences).
Intrinsic GFP expression from the *Hes5::GFP* reporter was assessed by flow cytometry by pelleting $1x10^6$ hESCs or rosette NSCs per condition, washing twice with DBPS, and resuspending in FACS buffer containing 100 ng of DAPI for dead cell exclusion. Samples were run and analyzed as described above.

Whole genome sequencing and pseudokaryotype generation

Genomic DNA was extracted from freshly harvested $5x10^6$ hESCs per condition using the DNeasy (Qiagen) DNA collection kit according to the manufacturer's protocol. Whole-genome libraries were prepared by the NYU Genome Technology Center using the Illumina DNA Prep PCR-Free Library Kit and sequenced on an Illumina NovaSeq X with a target of 50X genomic coverage. Demultiplexed fastq files were trimmed of adapters and filtered of low-quality reads using Trim Galore with Phred quality scores below 20. Reads were aligned against the UCSC HS1 telomere-to-telomere human genome using Bowtie2 to generate BAM files, and duplicates were removed using picard tools. The resulting BAM files were used to create BigWig files utilizing deeptools with 500 kb binning for purposes of pseudokaryotypes or 10 bp binning for CRISPR target deletion confirmation.[83] Pseudokaryotypes were generated from BigWig files using Karyoploter.[96]

Western blot

10 million cells per condition were lysed in RIPA buffer (Thermo Fisher) supplemented with Halt protease inhibitor cocktail (Thermo Fisher). Samples were incubated on ice for 10 min and then sonicated in a water-bath Bioruptor (Diagenode) at medium power setting for 10 cycles of 15 s "On" and 60 s "Off" at 4 °C. Lysates were centrifuged at 15,000xg for 10 min at 4 °C. Protein concentrations were determined using the DC protein assay kit II (Bio-Rad). Laemmli buffer (Bio-Rad) containing β-mercaptoethanol was then added to protein lysates. Samples were incubated at 95 °C for 5 min. Twenty μg of protein per sample were loaded onto SDS-PAGE gels for separation and transferred to 0.2 μm nitrocellulose membranes (Bio-Rad). After blocking the membranes in 2% bovine serum albumin (BSA) in TBS-Tween for 1 h at RT, they were simultaneously incubated with antibodies against SOX2 (R&D Systems) or β-Actin at 1:200 and 1:1000, respectively. Blots were incubated at 4 °C overnight and visualized with two simultaneous fluorescent Alexa Fluor Plus–conjugated secondary antibodies. Images were acquired using the iBright FL1000 system (Invitrogen). Densitometric quantification of band intensities was conducted in ImageJ.

887 **Immunofluorescence microscopy**
888 Cell cultures were fixed with 4% paraformaldehyde (PFA) for 30 min at RT, followed by block and
889 permeabilization with 10% bovine serum albumin (BSA) in PBS supplemented with 0.1% Triton X-100 for
890 1 h at RT. Cells were then incubated with primary antibodies (Table 4) in 1% BSA in PBS + 0.1% Triton X-
891 100 at 4°C overnight. The next day, cells were washed with PBS + 0.1% Triton X-100 and stained with
892 donkey AlexaPlus IgG (H+L) secondary antibodies for 1 h at RT. Nuclei were counterstained with 500
893 ng/mL 4′,6-diamidino-2-phenylindole (DAPI) for 10 min at RT. Microscopy was conducted on a Zeiss Axio-
894 observer microscope.
895
896 **Teratoma tissue harvesting, sectioning, and staining**
897 Each teratoma was partially dissected to obtain small samples for flash freezing and cryopreservation for
898 downstream analysis by sequencing assays. The remaining teratoma tissue was immediately transferred
899 to 4% PFA and incubated at 4 °C for 24 hours. Samples were then transferred to 20% sucrose to dehydrate
900 overnight at 4 °C. After tissue dehydration was complete, samples were embedded into optimal cutting
901 temperature (OCT) medium, mounted onto cutting blocks, and cryosectioned at 20 μm thickness onto glass
902 slides. Slides were immediately transferred to -20°C for storage until immunostaining, which was performed
903 as described above, or H&E staining.
904
905 **Tissue clearing and immunostaining of cerebral organoids**
906 Cerebral organoids were cleared and immunostained as previously published.[97] In brief, organoids were
907 fixed in 4% PFA and then incubated in PBS with 0.1% Tween-20. Organoids were washed with organoid
908 wash buffer (PBS, 0.1% Triton X-100, 0.2% BSA) and blocked at RT. They were then incubated with primary
909 antibodies (Table 4) for 24 hours at 4°C. Following primary antibody incubation, organoids were washed 3
910 times for 2 hours per wash. They were then incubated with secondary antibodies [donkey AlexaPlus IgG
911 (H+L) diluted to 1:500 in organoid wash buffer] for 24 hours at 4 °C. After 3 washes with organoid wash
912 buffer (2 hours per wash), they were stained with 500 ng/mL DAPI. Organoids were then gently centrifuged
913 at 70xg for 3 minutes and resuspended in 150 μL of FocusClear (CelExplorer Labs) for 1 hour or until
914 visually clarified. Organoids were then mounted in 40 μL of FocusClear on glass slides with glass #1
915 coverslips (Fisherbrand) and imaged on a Zeiss LSM800 confocal microscope.
916
917 **Quantification and statistical analysis**
918 Statistical analysis was performed using GraphPad Prism (version 8.4.3). Population statistics are
919 represented as mean ± standard error of the mean (SEM) throughout. Statistical significance was calculated
920 using Student's t-test, one-way analysis of variance (ANOVA) or two-way ANOVA with Tukey's and Sidak's
921 *post hoc* test for multiple comparisons, $\chi 2$ for trend and Benjamini-Hochberg multiple testing procedure. P
922 values <0.05 were considered statistically significant (*p<0.05; **p<0.01; ***p<0.001). For GO term
923 statistical analysis of scRNA-seq data, differential expression (DE) testing was based on the non-parametric
924 Wilcoxon rank sum test with multiple comparison correction by FDR (False Discovery Rate).
925

REFERENCES

1. Vaquerizas, J.M., Kummerfeld, S.K., Teichmann, S.A., and Luscombe, N.M. (2009). A census of human transcription factors: function, expression and evolution. Nat Rev Genet *10*, 252-263. 10.1038/nrg2538.
2. Accili, D., and Arden, K.C. (2004). FoxOs at the crossroads of cellular metabolism, differentiation, and transformation. Cell *117*, 421-426. 10.1016/s0092-8674(04)00452-0.
3. Gabriele, M., Brandao, H.B., Grosse-Holz, S., Jha, A., Dailey, G.M., Cattoglio, C., Hsieh, T.S., Mirny, L., Zechner, C., and Hansen, A.S. (2022). Dynamics of CTCF- and cohesin-mediated chromatin looping revealed by live-cell imaging. Science *376*, 496-501. 10.1126/science.abn6583.
4. Beagan, J.A., and Phillips-Cremins, J.E. (2020). On the existence and functionality of topologically associating domains. Nat Genet *52*, 8-16. 10.1038/s41588-019-0561-1.
5. Sanborn, A.L., Rao, S.S., Huang, S.C., Durand, N.C., Huntley, M.H., Jewett, A.I., Bochkov, I.D., Chinnappan, D., Cutkosky, A., Li, J., et al. (2015). Chromatin extrusion explains key features of loop and domain formation in wild-type and engineered genomes. Proc Natl Acad Sci U S A *112*, E6456-6465. 10.1073/pnas.1518552112.
6. Fudenberg, G., Imakaev, M., Lu, C., Goloborodko, A., Abdennur, N., and Mirny, L.A. (2016). Formation of Chromosomal Domains by Loop Extrusion. Cell Rep *15*, 2038-2049. 10.1016/j.celrep.2016.04.085.
7. Kim, K.L., Rahme, G.J., Goel, V.Y., El Farran, C.A., Hansen, A.S., and Bernstein, B.E. (2024). Dissection of a CTCF topological boundary uncovers principles of enhancer-oncogene regulation. Mol Cell *84*, 1365-1376 e1367. 10.1016/j.molcel.2024.02.007.
8. Bowles, J., Schepers, G., and Koopman, P. (2000). Phylogeny of the SOX family of developmental transcription factors based on sequence and structural indicators. Dev Biol *227*, 239-255. 10.1006/dbio.2000.9883.
9. Stevanovic, M., Zuffardi, O., Collignon, J., Lovell-Badge, R., and Goodfellow, P. (1994). The cDNA sequence and chromosomal location of the human SOX2 gene. Mamm Genome *5*, 640-642. 10.1007/BF00411460.
10. Thomson, M., Liu, S.J., Zou, L.N., Smith, Z., Meissner, A., and Ramanathan, S. (2011). Pluripotency factors in embryonic stem cells regulate differentiation into germ layers. Cell *145*, 875-889. 10.1016/j.cell.2011.05.017.
11. Li, Y., Rivera, C.M., Ishii, H., Jin, F., Selvaraj, S., Lee, A.Y., Dixon, J.R., and Ren, B. (2014). CRISPR reveals a distal super-enhancer required for Sox2 expression in mouse embryonic stem cells. PLoS One *9*, e114485. 10.1371/journal.pone.0114485.
12. Chew, J.L., Loh, Y.H., Zhang, W., Chen, X., Tam, W.L., Yeap, L.S., Li, P., Ang, Y.S., Lim, B., Robson, P., and Ng, H.H. (2005). Reciprocal transcriptional regulation of Pou5f1 and Sox2 via the Oct4/Sox2 complex in embryonic stem cells. Mol Cell Biol *25*, 6031-6046. 10.1128/MCB.25.14.6031-6046.2005.
13. Rodda, D.J., Chew, J.L., Lim, L.H., Loh, Y.H., Wang, B., Ng, H.H., and Robson, P. (2005). Transcriptional regulation of nanog by OCT4 and SOX2. J Biol Chem *280*, 24731-24737. 10.1074/jbc.M502573200.
14. Avilion, A.A., Nicolis, S.K., Pevny, L.H., Perez, L., Vivian, N., and Lovell-Badge, R. (2003). Multipotent cell lineages in early mouse development depend on SOX2 function. Genes Dev *17*, 126-140. 10.1101/gad.224503.
15. Zhou, C., Yang, X., Sun, Y., Yu, H., Zhang, Y., and Jin, Y. (2016). Comprehensive profiling reveals mechanisms of SOX2-mediated cell fate specification in human ESCs and NPCs. Cell Res *26*, 171-189. 10.1038/cr.2016.15.
16. Que, J., Luo, X., Schwartz, R.J., and Hogan, B.L. (2009). Multiple roles for Sox2 in the developing and adult mouse trachea. Development *136*, 1899-1907. 10.1242/dev.034629.
17. Sarkar, A., and Hochedlinger, K. (2013). The sox family of transcription factors: versatile regulators of stem and progenitor cell fate. Cell Stem Cell *12*, 15-30. 10.1016/j.stem.2012.12.007.
18. Cavallaro, M., Mariani, J., Lancini, C., Latorre, E., Caccia, R., Gullo, F., Valotta, M., DeBiasi, S., Spinardi, L., Ronchi, A., et al. (2008). Impaired generation of mature neurons by neural stem cells from hypomorphic Sox2 mutants. Development *135*, 541-557. 10.1242/dev.010801.
19. Ferri, A.L., Cavallaro, M., Braida, D., Di Cristofano, A., Canta, A., Vezzani, A., Ottolenghi, S., Pandolfi, P.P., Sala, M., DeBiasi, S., and Nicolis, S.K. (2004). Sox2 deficiency causes

981 neurodegeneration and impaired neurogenesis in the adult mouse brain. Development *131*, 3805-
982 3819. 10.1242/dev.01204.
983 20. Miyagi, S., Masui, S., Niwa, H., Saito, T., Shimazaki, T., Okano, H., Nishimoto, M., Muramatsu, M.,
984 Iwama, A., and Okuda, A. (2008). Consequence of the loss of Sox2 in the developing brain of the
985 mouse. FEBS Lett *582*, 2811-2815. 10.1016/j.febslet.2008.07.011.
986 21. Amador-Arjona, A., Cimadamore, F., Huang, C.T., Wright, R., Lewis, S., Gage, F.H., and Terskikh,
987 A.V. (2015). SOX2 primes the epigenetic landscape in neural precursors enabling proper gene
988 activation during hippocampal neurogenesis. Proc Natl Acad Sci U S A *112*, E1936-1945.
989 10.1073/pnas.1421480112.
990 22. Lodato, M.A., Ng, C.W., Wamstad, J.A., Cheng, A.W., Thai, K.K., Fraenkel, E., Jaenisch, R., and
991 Boyer, L.A. (2013). SOX2 co-occupies distal enhancer elements with distinct POU factors in ESCs
992 and NPCs to specify cell state. PLoS Genet *9*, e1003288. 10.1371/journal.pgen.1003288.
993 23. Suh, H., Consiglio, A., Ray, J., Sawai, T., D'Amour, K.A., and Gage, F.H. (2007). In vivo fate
994 analysis reveals the multipotent and self-renewal capacities of Sox2+ neural stem cells in the adult
995 hippocampus. Cell Stem Cell *1*, 515-528. 10.1016/j.stem.2007.09.002.
996 24. Zhang, S., and Cui, W. (2014). Sox2, a key factor in the regulation of pluripotency and neural
997 differentiation. World J Stem Cells *6*, 305-311. 10.4252/wjsc.v6.i3.305.
998 25. Bertolini, J.A., Favaro, R., Zhu, Y., Pagin, M., Ngan, C.Y., Wong, C.H., Tjong, H., Vermunt, M.W.,
999 Martynoga, B., Barone, C., et al. (2019). Mapping the Global Chromatin Connectivity Network for
1000 Sox2 Function in Neural Stem Cell Maintenance. Cell Stem Cell *24*, 462-476 e466.
1001 10.1016/j.stem.2019.02.004.
1002 26. Zhang, S., Bell, E., Zhi, H., Brown, S., Imran, S.A.M., Azuara, V., and Cui, W. (2019). OCT4 and
1003 PAX6 determine the dual function of SOX2 in human ESCs as a key pluripotent or neural factor.
1004 Stem Cell Res Ther *10*, 122. 10.1186/s13287-019-1228-7.
1005 27. Annovazzi, L., Mellai, M., Caldera, V., Valente, G., and Schiffer, D. (2011). SOX2 expression and
1006 amplification in gliomas and glioma cell lines. Cancer Genomics Proteomics *8*, 139-147.
1007 28. Bulstrode, H., Johnstone, E., Marques-Torrejon, M.A., Ferguson, K.M., Bressan, R.B., Blin, C.,
1008 Grant, V., Gogolok, S., Gangoso, E., Gagrica, S., et al. (2017). Elevated FOXG1 and SOX2 in
1009 glioblastoma enforces neural stem cell identity through transcriptional control of cell cycle and
1010 epigenetic regulators. Genes Dev *31*, 757-773. 10.1101/gad.293027.116.
1011 29. Rudin, C.M., Durinck, S., Stawiski, E.W., Poirier, J.T., Modrusan, Z., Shames, D.S., Bergbower,
1012 E.A., Guan, Y., Shin, J., Guillory, J., et al. (2012). Comprehensive genomic analysis identifies SOX2
1013 as a frequently amplified gene in small-cell lung cancer. Nat Genet *44*, 1111-1116.
1014 10.1038/ng.2405.
1015 30. Alexander, J.M., Guan, J., Li, B., Maliskova, L., Song, M., Shen, Y., Huang, B., Lomvardas, S., and
1016 Weiner, O.D. (2019). Live-cell imaging reveals enhancer-dependent Sox2 transcription in the
1017 absence of enhancer proximity. Elife *8*. 10.7554/eLife.41769.
1018 31. Liu, Z., Legant, W.R., Chen, B.C., Li, L., Grimm, J.B., Lavis, L.D., Betzig, E., and Tjian, R. (2014).
1019 3D imaging of Sox2 enhancer clusters in embryonic stem cells. Elife *3*, e04236.
1020 10.7554/eLife.04236.
1021 32. Miyagi, S., Nishimoto, M., Saito, T., Ninomiya, M., Sawamoto, K., Okano, H., Muramatsu, M.,
1022 Oguro, H., Iwama, A., and Okuda, A. (2006). The Sox2 regulatory region 2 functions as a neural
1023 stem cell-specific enhancer in the telencephalon. J Biol Chem *281*, 13374-13381.
1024 10.1074/jbc.M512669200.
1025 33. Tobias, I.C., Moorthy, S.D., Shchuka, V.M., Langroudi, L., Cherednychenko, M., Gillespie, Z.E.,
1026 Duncan, A.G., Tian, R., Gajewska, N.A., Di Roberto, R.B., and Mitchell, J.A. (2025). A Sox2
1027 enhancer cluster regulates region-specific neural fates from mouse embryonic stem cells. G3
1028 (Bethesda) *15*. 10.1093/g3journal/jkaf012.
1029 34. Shahzad, U., Nikolopoulos, M., Li, C., Johnston, M., Wang, J.J., Sabha, N., Varn, F.S.,
1030 Riemenschneider, A., Krumholtz, S., Krishnamurthy, P.M., et al. (2025). CASCADES, a novel
1031 SOX2 super-enhancer-associated long noncoding RNA, regulates cancer stem cell specification
1032 and differentiation in glioblastoma. Mol Oncol *19*, 764-784. 10.1002/1878-0261.13735.
1033 35. Tsaytler, P., Blaess, G., Scholze-Wittler, M., Koch, F., and Herrmann, B.G. (2024). Early neural
1034 specification of stem cells is mediated by a set of SOX2-dependent neural-associated enhancers.
1035 Stem Cell Reports *19*, 618-628. 10.1016/j.stemcr.2024.03.003.

36. Chakraborty, S., Kopitchinski, N., Zuo, Z., Eraso, A., Awasthi, P., Chari, R., Mitra, A., Tobias, I.C., Moorthy, S.D., Dale, R.K., et al. (2023). Enhancer-promoter interactions can bypass CTCF-mediated boundaries and contribute to phenotypic robustness. Nat Genet *55*, 280-290. 10.1038/s41588-022-01295-6.
37. Zhou, H.Y., Katsman, Y., Dhaliwal, N.K., Davidson, S., Macpherson, N.N., Sakthidevi, M., Collura, F., and Mitchell, J.A. (2014). A Sox2 distal enhancer cluster regulates embryonic stem cell differentiation potential. Genes Dev *28*, 2699-2711. 10.1101/gad.248526.114.
38. Modrek, A.S., Golub, D., Khan, T., Bready, D., Prado, J., Bowman, C., Deng, J., Zhang, G., Rocha, P.P., Raviram, R., et al. (2017). Low-Grade Astrocytoma Mutations in IDH1, P53, and ATRX Cooperate to Block Differentiation of Human Neural Stem Cells via Repression of SOX2. Cell Rep *21*, 1267-1280. 10.1016/j.celrep.2017.10.009.
39. Roadmap Epigenomics, C., Kundaje, A., Meuleman, W., Ernst, J., Bilenky, M., Yen, A., Heravi-Moussavi, A., Kheradpour, P., Zhang, Z., Wang, J., et al. (2015). Integrative analysis of 111 reference human epigenomes. Nature *518*, 317-330. 10.1038/nature14248.
40. Zhang, Y., Li, T., Preissl, S., Amaral, M.L., Grinstein, J.D., Farah, E.N., Destici, E., Qiu, Y., Hu, R., Lee, A.Y., et al. (2019). Transcriptionally active HERV-H retrotransposons demarcate topologically associating domains in human pluripotent stem cells. Nat Genet *51*, 1380-1388. 10.1038/s41588-019-0479-7.
41. Visel, A., Minovitsky, S., Dubchak, I., and Pennacchio, L.A. (2007). VISTA Enhancer Browser--a database of tissue-specific human enhancers. Nucleic Acids Res *35*, D88-92. 10.1093/nar/gkl822.
42. Lee, H.J., Hou, Y., Maeng, J.H., Shah, N.M., Chen, Y., Lawson, H.A., Yang, H., Yue, F., and Wang, T. (2022). Epigenomic analysis reveals prevalent contribution of transposable elements to cis-regulatory elements, tissue-specific expression, and alternative promoters in zebrafish. Genome Res *32*, 1424-1436. 10.1101/gr.276052.121.
43. Placantonakis, D.G., Tomishima, M.J., Lafaille, F., Desbordes, S.C., Jia, F., Socci, N.D., Viale, A., Lee, H., Harrison, N., Tabar, V., and Studer, L. (2009). BAC transgenesis in human embryonic stem cells as a novel tool to define the human neural lineage. Stem Cells *27*, 521-532. 10.1634/stemcells.2008-0884.
44. International Stem Cell, I. (2018). Assessment of established techniques to determine developmental and malignant potential of human pluripotent stem cells. Nat Commun *9*, 1925. 10.1038/s41467-018-04011-3.
45. Ng, E.S., Davis, R., Stanley, E.G., and Elefanty, A.G. (2008). A protocol describing the use of a recombinant protein-based, animal product-free medium (APEL) for human embryonic stem cell differentiation as spin embryoid bodies. Nat Protoc *3*, 768-776. 10.1038/nprot.2008.42.
46. Elkabetz, Y., Panagiotakos, G., Al Shamy, G., Socci, N.D., Tabar, V., and Studer, L. (2008). Human ES cell-derived neural rosettes reveal a functionally distinct early neural stem cell stage. Genes Dev *22*, 152-165. 10.1101/gad.1616208.
47. Tabar, V., Panagiotakos, G., Greenberg, E.D., Chan, B.K., Sadelain, M., Gutin, P.H., and Studer, L. (2005). Migration and differentiation of neural precursors derived from human embryonic stem cells in the rat brain. Nat Biotechnol *23*, 601-606. 10.1038/nbt1088.
48. McDonald, D., Wu, Y., Dailamy, A., Tat, J., Parekh, U., Zhao, D., Hu, M., Tipps, A., Zhang, K., and Mali, P. (2020). Defining the Teratoma as a Model for Multi-lineage Human Development. Cell *183*, 1402-1419 e1418. 10.1016/j.cell.2020.10.018.
49. Ge, S.X., Jung, D., and Yao, R. (2020). ShinyGO: a graphical gene-set enrichment tool for animals and plants. Bioinformatics *36*, 2628-2629. 10.1093/bioinformatics/btz931.
50. Toresson, H., Martinez-Barbera, J.P., Bardsley, A., Caubit, X., and Krauss, S. (1998). Conservation of BF-1 expression in amphioxus and zebrafish suggests evolutionary ancestry of anterior cell types that contribute to the vertebrate telencephalon. Dev Genes Evol *208*, 431-439. 10.1007/s004270050200.
51. Xuan, S., Baptista, C.A., Balas, G., Tao, W., Soares, V.C., and Lai, E. (1995). Winged helix transcription factor BF-1 is essential for the development of the cerebral hemispheres. Neuron *14*, 1141-1152. 10.1016/0896-6273(95)90262-7.
52. Cecchi, C. (2002). Emx2: a gene responsible for cortical development, regionalization and area specification. Gene *291*, 1-9. 10.1016/s0378-1119(02)00623-6.

53. Simeone, A., Acampora, D., Gulisano, M., Stornaiuolo, A., and Boncinelli, E. (1992). Nested expression domains of four homeobox genes in developing rostral brain. Nature *358*, 687-690. 10.1038/358687a0.
54. Chambers, S.M., Fasano, C.A., Papapetrou, E.P., Tomishima, M., Sadelain, M., and Studer, L. (2009). Highly efficient neural conversion of human ES and iPS cells by dual inhibition of SMAD signaling. Nat Biotechnol *27*, 275-280. 10.1038/nbt.1529.
55. Lancaster, M.A., Renner, M., Martin, C.A., Wenzel, D., Bicknell, L.S., Hurles, M.E., Homfray, T., Penninger, J.M., Jackson, A.P., and Knoblich, J.A. (2013). Cerebral organoids model human brain development and microcephaly. Nature *501*, 373-379. 10.1038/nature12517.
56. Pasca, S.P., Arlotta, P., Bateup, H.S., Camp, J.G., Cappello, S., Gage, F.H., Knoblich, J.A., Kriegstein, A.R., Lancaster, M.A., Ming, G.L., et al. (2025). A framework for neural organoids, assembloids and transplantation studies. Nature *639*, 315-320. 10.1038/s41586-024-08487-6.
57. Trevino, A.E., Sinnott-Armstrong, N., Andersen, J., Yoon, S.J., Huber, N., Pritchard, J.K., Chang, H.Y., Greenleaf, W.J., and Pasca, S.P. (2020). Chromatin accessibility dynamics in a model of human forebrain development. Science *367*. 10.1126/science.aay1645.
58. Velasco, S., Kedaigle, A.J., Simmons, S.K., Nash, A., Rocha, M., Quadrato, G., Paulsen, B., Nguyen, L., Adiconis, X., Regev, A., et al. (2019). Individual brain organoids reproducibly form cell diversity of the human cerebral cortex. Nature *570*, 523-527. 10.1038/s41586-019-1289-x.
59. Wang, D., Liu, S., Warrell, J., Won, H., Shi, X., Navarro, F.C.P., Clarke, D., Gu, M., Emani, P., Yang, Y.T., et al. (2018). Comprehensive functional genomic resource and integrative model for the human brain. Science *362*. 10.1126/science.aat8464.
60. Bryois, J., Garrett, M.E., Song, L., Safi, A., Giusti-Rodriguez, P., Johnson, G.D., Shieh, A.W., Buil, A., Fullard, J.F., Roussos, P., et al. (2018). Evaluation of chromatin accessibility in prefrontal cortex of individuals with schizophrenia. Nat Commun *9*, 3121. 10.1038/s41467-018-05379-y.
61. Wang, Y., Zhang, S., Lan, Z., Doan, V., Kim, B., Liu, S., Zhu, M., Hull, V.L., Rihani, S., Zhang, C.L., et al. (2022). SOX2 is essential for astrocyte maturation and its deletion leads to hyperactive behavior in mice. Cell Rep *41*, 111842. 10.1016/j.celrep.2022.111842.
62. Zemke, N.R., Armand, E.J., Wang, W., Lee, S., Zhou, J., Li, Y.E., Liu, H., Tian, W., Nery, J.R., Castanon, R.G., et al. (2024). Author Correction: Conserved and divergent gene regulatory programs of the mammalian neocortex. Nature *625*, E26. 10.1038/s41586-023-07013-4.
63. Nord, A.S., and West, A.E. (2020). Neurobiological functions of transcriptional enhancers. Nat Neurosci *23*, 5-14. 10.1038/s41593-019-0538-5.
64. Bani-Yaghoub, M., Tremblay, R.G., Lei, J.X., Zhang, D., Zurakowski, B., Sandhu, J.K., Smith, B., Ribecco-Lutkiewicz, M., Kennedy, J., Walker, P.R., and Sikorska, M. (2006). Role of Sox2 in the development of the mouse neocortex. Dev Biol *295*, 52-66. 10.1016/j.ydbio.2006.03.007.
65. Favaro, R., Valotta, M., Ferri, A.L., Latorre, E., Mariani, J., Giachino, C., Lancini, C., Tosetti, V., Ottolenghi, S., Taylor, V., and Nicolis, S.K. (2009). Hippocampal development and neural stem cell maintenance require Sox2-dependent regulation of Shh. Nat Neurosci *12*, 1248-1256. 10.1038/nn.2397.
66. Graham, V., Khudyakov, J., Ellis, P., and Pevny, L. (2003). SOX2 functions to maintain neural progenitor identity. Neuron *39*, 749-765. 10.1016/s0896-6273(03)00497-5.
67. Karr, J.P., Ferrie, J.J., Tjian, R., and Darzacq, X. (2022). The transcription factor activity gradient (TAG) model: contemplating a contact-independent mechanism for enhancer-promoter communication. Genes Dev *36*, 7-16. 10.1101/gad.349160.121.
68. Blackburn, P.R., Chacon-Camacho, O.F., Ortiz-Gonzalez, X.R., Reyes, M., Lopez-Uriarte, G.A., Zarei, S., Bhoj, E.J., Perez-Solorzano, S., Vaubel, R.A., Murphree, M.I., et al. (2018). Extension of the mutational and clinical spectrum of SOX2 related disorders: Description of six new cases and a novel association with suprasellar teratoma. Am J Med Genet A *176*, 2710-2719. 10.1002/ajmg.a.40644.
69. Fantes, J., Ragge, N.K., Lynch, S.A., McGill, N.I., Collin, J.R., Howard-Peebles, P.N., Hayward, C., Vivian, A.J., Williamson, K., van Heyningen, V., and FitzPatrick, D.R. (2003). Mutations in SOX2 cause anophthalmia. Nat Genet *33*, 461-463. 10.1038/ng1120.
70. Ragge, N.K., Lorenz, B., Schneider, A., Bushby, K., de Sanctis, L., de Sanctis, U., Salt, A., Collin, J.R., Vivian, A.J., Free, S.L., et al. (2005). SOX2 anophthalmia syndrome. Am J Med Genet A *135*, 1-7; discussion 8. 10.1002/ajmg.a.30642.

71. Shoichet, S.A., Kunde, S.A., Viertel, P., Schell-Apacik, C., von Voss, H., Tommerup, N., Ropers, H.H., and Kalscheuer, V.M. (2005). Haploinsufficiency of novel FOXG1B variants in a patient with severe mental retardation, brain malformations and microcephaly. Hum Genet *117*, 536-544. 10.1007/s00439-005-1310-3.
72. Avantaggiato, V., Pandolfi, P.P., Ruthardt, M., Hawe, N., Acampora, D., Pelicci, P.G., and Simeone, A. (1995). Developmental analysis of murine Promyelocyte Leukemia Zinc Finger (PLZF) gene expression: implications for the neuromeric model of the forebrain organization. J Neurosci *15*, 4927-4942. 10.1523/JNEUROSCI.15-07-04927.1995.
73. Dixon, J.R., Jung, I., Selvaraj, S., Shen, Y., Antosiewicz-Bourget, J.E., Lee, A.Y., Ye, Z., Kim, A., Rajagopal, N., Xie, W., et al. (2015). Chromatin architecture reorganization during stem cell differentiation. Nature *518*, 331-336. 10.1038/nature14222.
74. Bonev, B., Mendelson Cohen, N., Szabo, Q., Fritsch, L., Papadopoulos, G.L., Lubling, Y., Xu, X., Lv, X., Hugnot, J.P., Tanay, A., and Cavalli, G. (2017). Multiscale 3D Genome Rewiring during Mouse Neural Development. Cell *171*, 557-572 e524. 10.1016/j.cell.2017.09.043.
75. Yang, H., Luan, Y., Liu, T., Lee, H.J., Fang, L., Wang, Y., Wang, X., Zhang, B., Jin, Q., Ang, K.C., et al. (2020). A map of cis-regulatory elements and 3D genome structures in zebrafish. Nature *588*, 337-343. 10.1038/s41586-020-2962-9.
76. Hu, B., Won, H., Mah, W., Park, R.B., Kassim, B., Spiess, K., Kozlenkov, A., Crowley, C.A., Pochareddy, S., Psych, E.C., et al. (2021). Neuronal and glial 3D chromatin architecture informs the cellular etiology of brain disorders. Nat Commun *12*, 3968. 10.1038/s41467-021-24243-0.
77. Vidigal, J.A., and Ventura, A. (2015). Rapid and efficient one-step generation of paired gRNA CRISPR-Cas9 libraries. Nat Commun *6*, 8083. 10.1038/ncomms9083.
78. Amit, M., Carpenter, M.K., Inokuma, M.S., Chiu, C.P., Harris, C.P., Waknitz, M.A., Itskovitz-Eldor, J., and Thomson, J.A. (2000). Clonally derived human embryonic stem cell lines maintain pluripotency and proliferative potential for prolonged periods of culture. Dev Biol *227*, 271-278. 10.1006/dbio.2000.9912.
79. Frenster, J.D., and Placantonakis, D.G. (2018). Establishing Primary Human Glioblastoma Tumorsphere Cultures from Operative Specimens. Methods Mol Biol *1741*, 63-69. 10.1007/978-1-4939-7659-1_4.
80. Schmidl, C., Rendeiro, A.F., Sheffield, N.C., and Bock, C. (2015). ChIPmentation: fast, robust, low-input ChIP-seq for histones and transcription factors. Nat Methods *12*, 963-965. 10.1038/nmeth.3542.
81. Corces, M.R., Trevino, A.E., Hamilton, E.G., Greenside, P.G., Sinnott-Armstrong, N.A., Vesuna, S., Satpathy, A.T., Rubin, A.J., Montine, K.S., Wu, B., et al. (2017). An improved ATAC-seq protocol reduces background and enables interrogation of frozen tissues. Nat Methods *14*, 959-962. 10.1038/nmeth.4396.
82. Buenrostro, J.D., Wu, B., Chang, H.Y., and Greenleaf, W.J. (2015). ATAC-seq: A Method for Assaying Chromatin Accessibility Genome-Wide. Curr Protoc Mol Biol *109*, 21 29 21-21 29 29. 10.1002/0471142727.mb2129s109.
83. Ramirez, F., Dundar, F., Diehl, S., Gruning, B.A., and Manke, T. (2014). deepTools: a flexible platform for exploring deep-sequencing data. Nucleic Acids Res *42*, W187-191. 10.1093/nar/gku365.
84. Perez, G., Barber, G.P., Benet-Pages, A., Casper, J., Clawson, H., Diekhans, M., Fischer, C., Gonzalez, J.N., Hinrichs, A.S., Lee, C.M., et al. (2025). The UCSC Genome Browser database: 2025 update. Nucleic Acids Res *53*, D1243-D1249. 10.1093/nar/gkae974.
85. Hao, Y., Stuart, T., Kowalski, M.H., Choudhary, S., Hoffman, P., Hartman, A., Srivastava, A., Molla, G., Madad, S., Fernandez-Granda, C., and Satija, R. (2024). Dictionary learning for integrative, multimodal and scalable single-cell analysis. Nat Biotechnol *42*, 293-304. 10.1038/s41587-023-01767-y.
86. Zhang, Y., Liu, T., Meyer, C.A., Eeckhoute, J., Johnson, D.S., Bernstein, B.E., Nusbaum, C., Myers, R.M., Brown, M., Li, W., and Liu, X.S. (2008). Model-based analysis of ChIP-Seq (MACS). Genome Biol *9*, R137. 10.1186/gb-2008-9-9-r137.
87. Kloetgen, A., Thandapani, P., Ntziachristos, P., Ghebrechristos, Y., Nomikou, S., Lazaris, C., Chen, X., Hu, H., Bakogianni, S., Wang, J., et al. (2020). Three-dimensional chromatin landscapes in T cell acute lymphoblastic leukemia. Nat Genet *52*, 388-400. 10.1038/s41588-020-0602-9.

88. Raviram, R., Rocha, P.P., Muller, C.L., Miraldi, E.R., Badri, S., Fu, Y., Swanzey, E., Proudhon, C., Snetkova, V., Bonneau, R., and Skok, J.A. (2016). 4C-ker: A Method to Reproducibly Identify Genome-Wide Interactions Captured by 4C-Seq Experiments. PLoS Comput Biol *12*, e1004780. 10.1371/journal.pcbi.1004780.
89. Hershberg, E.A., Camplisson, C.K., Close, J.L., Attar, S., Chern, R., Liu, Y., Akilesh, S., Nicovich, P.R., and Beliveau, B.J. (2021). PaintSHOP enables the interactive design of transcriptome- and genome-scale oligonucleotide FISH experiments. Nat Methods *18*, 937-944. 10.1038/s41592-021-01187-3.
90. Fu, Y., Zhao, T., Clark, F., Nomikou, S., Tsirigos, A., and Lionnet, T. (2024). Connecting Chromatin Structures to Gene Regulation Using Dynamic Polymer Simulations. bioRxiv. 10.1101/2023.11.07.566032.
91. Mateo, L.J., Sinnott-Armstrong, N., and Boettiger, A.N. (2021). Tracing DNA paths and RNA profiles in cultured cells and tissues with ORCA. Nat Protoc *16*, 1647-1713. 10.1038/s41596-020-00478-x.
92. Zheng, M., Tian, S.Z., Capurso, D., Kim, M., Maurya, R., Lee, B., Piecuch, E., Gong, L., Zhu, J.J., Li, Z., et al. (2019). Multiplex chromatin interactions with single-molecule precision. Nature *566*, 558-562. 10.1038/s41586-019-0949-1.
93. Edelstein, A., Amodaj, N., Hoover, K., Vale, R., and Stuurman, N. (2010). Computer control of microscopes using microManager. Curr Protoc Mol Biol *Chapter 14*, Unit14 20. 10.1002/0471142727.mb1420s92.
94. Pachitariu, M., and Stringer, C. (2022). Cellpose 2.0: how to train your own model. Nat Methods *19*, 1634-1641. 10.1038/s41592-022-01663-4.
95. Lionnet, T., Czaplinski, K., Darzacq, X., Shav-Tal, Y., Wells, A.L., Chao, J.A., Park, H.Y., de Turris, V., Lopez-Jones, M., and Singer, R.H. (2011). A transgenic mouse for in vivo detection of endogenous labeled mRNA. Nat Methods *8*, 165-170. 10.1038/nmeth.1551.
96. Gel, B., and Serra, E. (2017). karyoploteR: an R/Bioconductor package to plot customizable genomes displaying arbitrary data. Bioinformatics *33*, 3088-3090. 10.1093/bioinformatics/btx346.
97. Dekkers, J.F., Alieva, M., Wellens, L.M., Ariese, H.C.R., Jamieson, P.R., Vonk, A.M., Amatngalim, G.D., Hu, H., Oost, K.C., Snippert, H.J.G., et al. (2019). High-resolution 3D imaging of fixed and cleared organoids. Nat Protoc *14*, 1756-1771. 10.1038/s41596-019-0160-8.

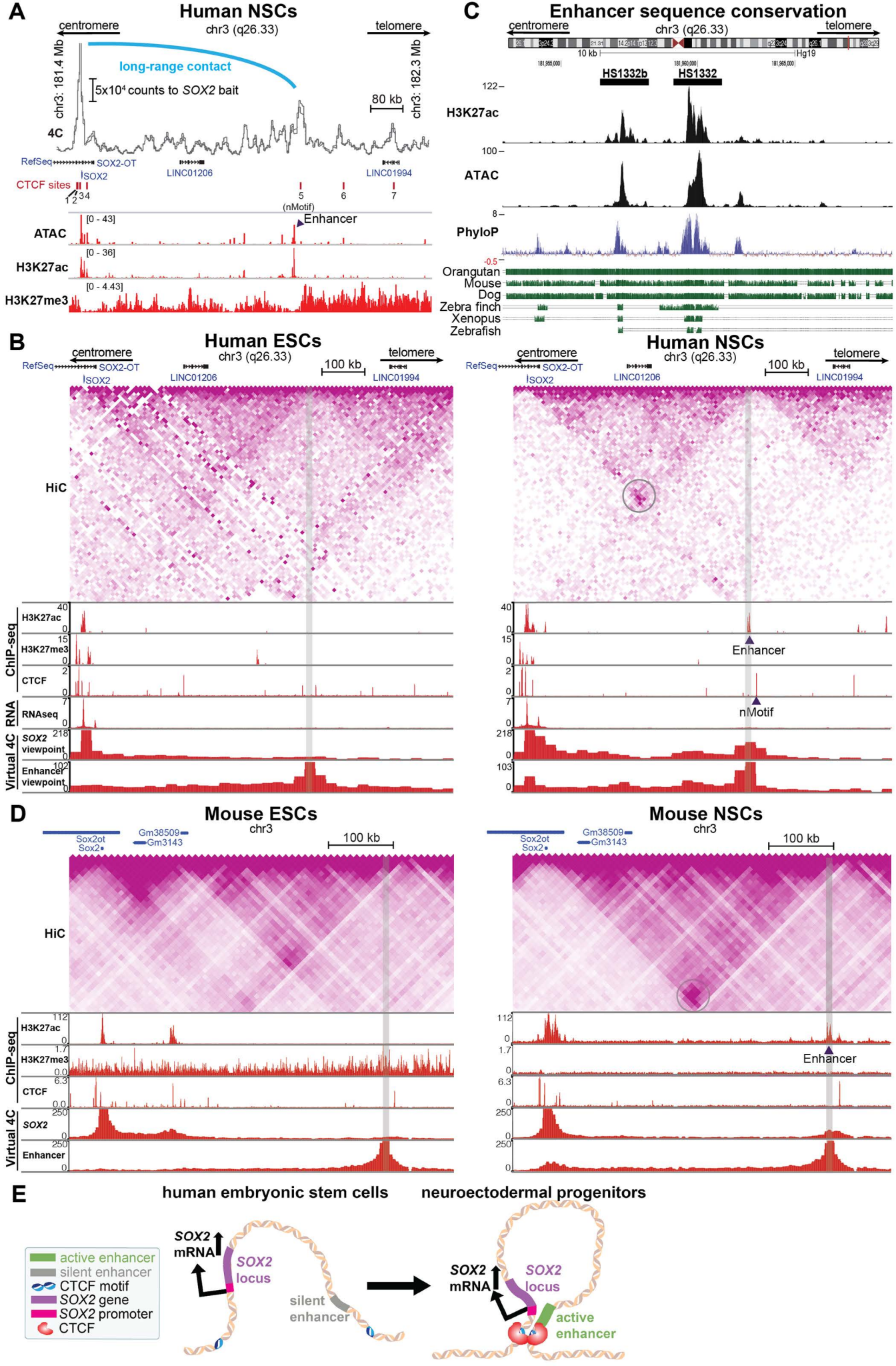
A
Human NSCs
centromere
chr3 (q26.33)
telomere
chr3: 181.4 Mb
chr3: 182.3 Mb
long-range contact
5x10⁴ counts to SOX2 bait
80 kb
4C
RefSeq
SOX2-OT
SOX2
LINC01206
LINC01994
CTCF sites
(nMotif)
Enhancer
ATAC
H3K27ac
H3K27me3
C
Enhancer sequence conservation
HS1332b
HS1332
H3K27ac
ATAC
PhyloP
Orangutan
Mouse
Dog
Zebra finch
Xenopus
Zebrafish
B
Human ESCs
Human NSCs
100 kb
HiC
ChIP-seq
H3K27ac
H3K27me3
CTCF
RNA
RNAseq
Virtual 4C
SOX2 viewpoint
Enhancer viewpoint
nMotif
D
Mouse ESCs
Mouse NSCs
chr3
Sox2ot
Sox2
Gm38509
Gm3143
E
human embryonic stem cells
neuroectodermal progenitors
active enhancer
silent enhancer
CTCF motif
SOX2 gene
SOX2 promoter
CTCF
SOX2 mRNA
SOX2 locus
silent enhancer
active enhancer

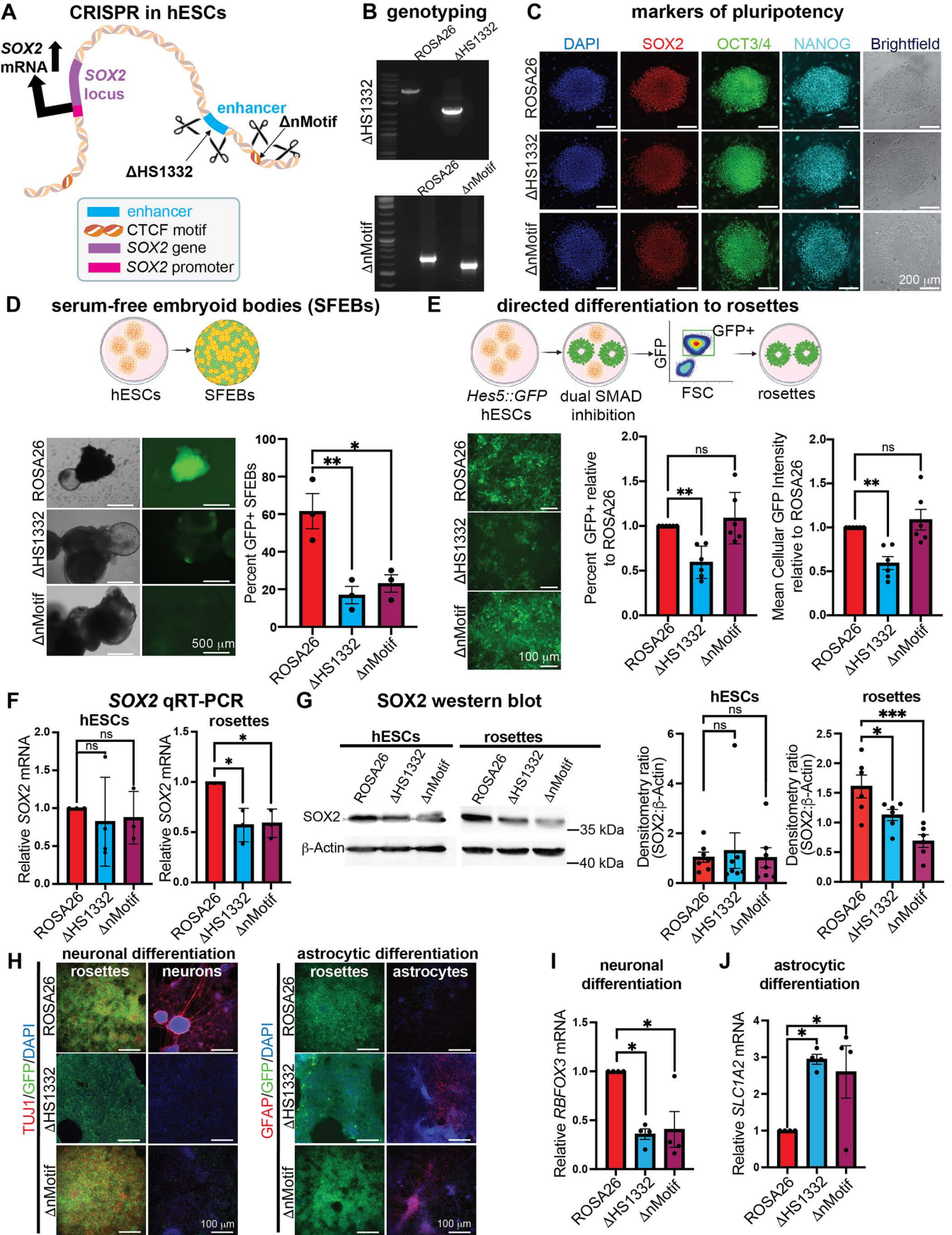
A
CRISPR in hESCs
SOX2 mRNA
SOX2 locus
enhancer
ΔnMotif
ΔHS1332
enhancer
CTCF motif
SOX2 gene
SOX2 promoter
B genotyping
ROSA26
ΔHS1332
ΔHS1332
ROSA26
ΔnMotif
ΔnMotif
C
markers of pluripotency
DAPI
SOX2
OCT3/4
NANOG
Brightfield
ROSA26
ΔHS1332
ΔnMotif
200 µm
D
serum-free embryoid bodies (SFEBs)
hESCs
SFEBs
ROSA26
ΔHS1332
ΔnMotif
500 µm
Percent GFP+ SFEBs
100
80
60
40
20
0
**
*
ROSA26
ΔHS1332
ΔnMotif
E
directed differentiation to rosettes
Hes5::GFP hESCs
dual SMAD inhibition
GFP
GFP+
FSC
rosettes
ROSA26
ΔHS1332
ΔnMotif
100 µm
Percent GFP+ relative to ROSA26
2.0
1.5
1.0
0.5
0.0
ns
**
ROSA26
ΔHS1332
ΔnMotif
Mean Cellular GFP Intensity relative to ROSA26
2.0
1.5
1.0
0.5
0.0
ns
**
ROSA26
ΔHS1332
ΔnMotif
F
SOX2 qRT-PCR
hESCs
rosettes
Relative SOX2 mRNA
2.0
1.5
1.0
0.5
0.0
ns
*
ROSA26
ΔHS1332
ΔnMotif
G
SOX2 western blot
hESCs
rosettes
ROSA26
ΔHS1332
ΔnMotif
ROSA26
ΔHS1332
ΔnMotif
SOX2
β-Actin
35 kDa
40 kDa
hESCs
Densitometry ratio (SOX2:β-Actin)
6
4
2
0
ns
ns
ROSA26
ΔHS1332
ΔnMotif
rosettes
Densitometry ratio (SOX2:β-Actin)
2.5
2.0
1.5
1.0
0.5
0.0
***
*
ROSA26
ΔHS1332
ΔnMotif
H
neuronal differentiation
rosettes
neurons
astrocytic differentiation
rosettes
astrocytes
TUJ1/GFP/DAPI
GFAP/GFP/DAPI
ROSA26
ΔHS1332
ΔnMotif
100 µm
100 µm
I
neuronal differentiation
Relative RBFOX3 mRNA
1.5
1.0
0.5
0.0
*
*
ROSA26
ΔHS1332
ΔnMotif
J
astrocytic differentiation
Relative SLC1A2 mRNA
4
3
2
1
0
*
*
ROSA26
ΔHS1332
ΔnMotif

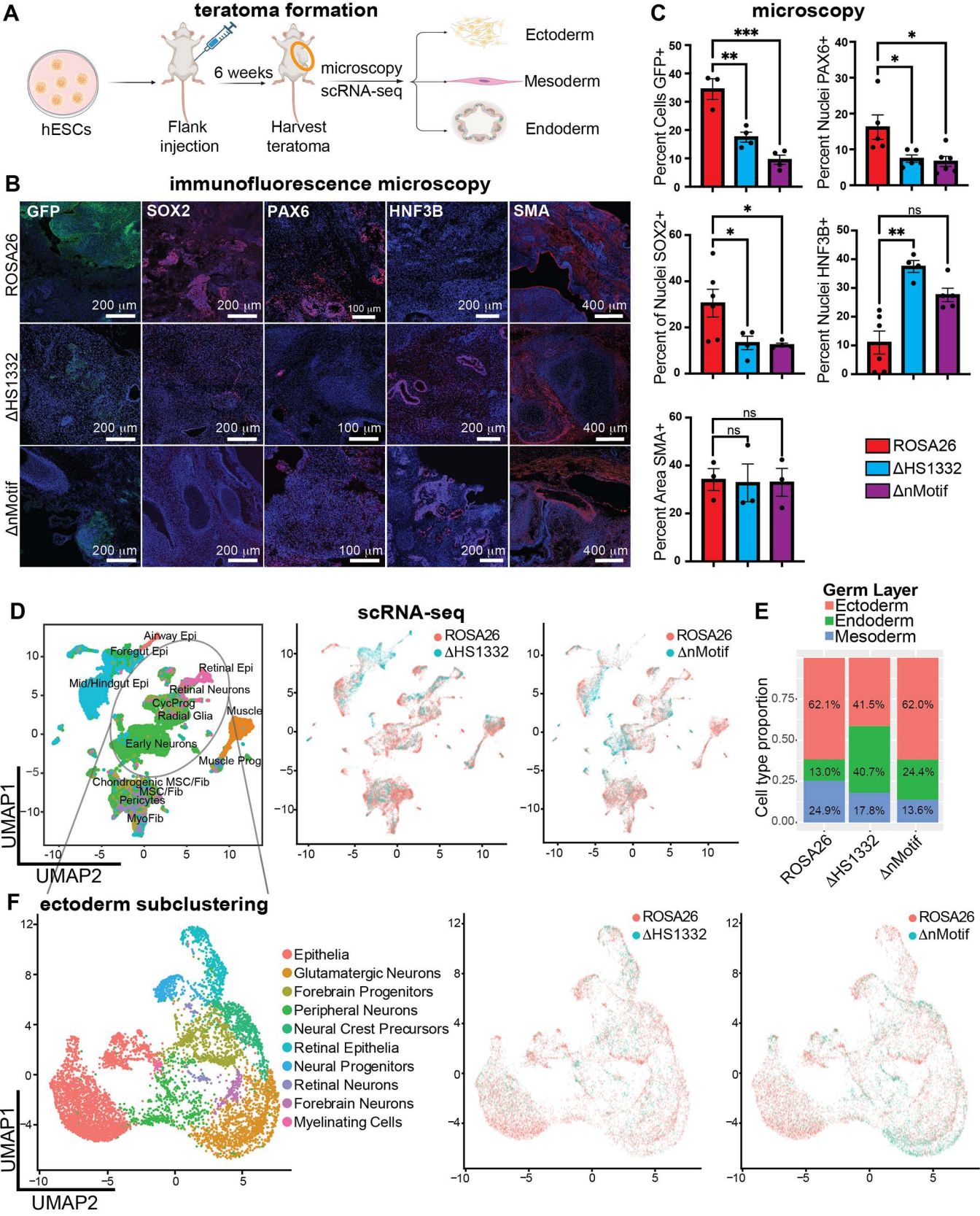
A
teratoma formation
hESCs
Flank injection
6 weeks
Harvest teratoma
microscopy
scRNA-seq
Ectoderm
Mesoderm
Endoderm
B
immunofluorescence microscopy
GFP
SOX2
PAX6
HNF3B
SMA
ROSA26
ΔHS1332
ΔnMotif
200 µm
100 µm
400 µm
C
microscopy
Percent Cells GFP+
Percent Nuclei PAX6+
Percent of Nuclei SOX2+
Percent Nuclei HNF3B+
Percent Area SMA+
ns
ROSA26
ΔHS1332
ΔnMotif
D
scRNA-seq
Airway Epi
Foregut Epi
Retinal Epi
Mid/Hindgut Epi
Retinal Neurons
CycProg
Radial Glia
Muscle
Early Neurons
Muscle Prog
Chondrogenic MSC/Fib
MSC/Fib
Pericytes
MyoFib
UMAP1
UMAP2
ROSA26
ΔHS1332
ΔnMotif
E
Germ Layer
Ectoderm
Endoderm
Mesoderm
Cell type proportion
62.1%
41.5%
62.0%
13.0%
40.7%
24.4%
24.9%
17.8%
13.6%
ROSA26
ΔHS1332
ΔnMotif
F
ectoderm subclustering
Epithelia
Glutamatergic Neurons
Forebrain Progenitors
Peripheral Neurons
Neural Crest Precursors
Retinal Epithelia
Neural Progenitors
Retinal Neurons
Forebrain Neurons
Myelinating Cells
UMAP1
UMAP2
ROSA26
ΔHS1332
ROSA26
ΔnMotif

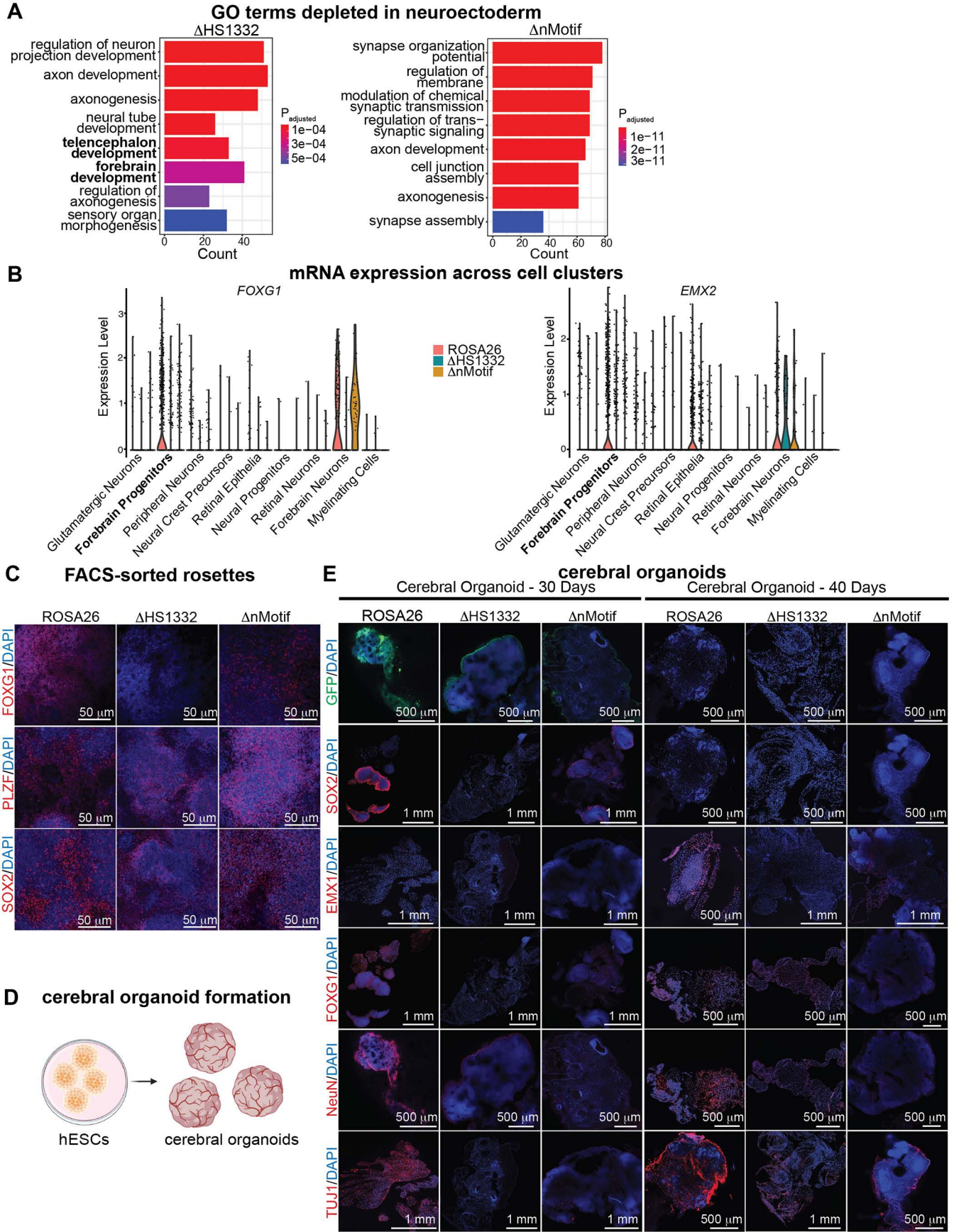
A
GO terms depleted in neuroectoderm
ΔHS1332
regulation of neuron projection development
axon development
axonogenesis
neural tube development
telencephalon development
forebrain development
regulation of axonogenesis
sensory organ morphogenesis
Count
P adjusted
1e−04
3e−04
5e−04
ΔnMotif
synapse organization potential
regulation of membrane
modulation of chemical synaptic transmission
regulation of trans−synaptic signaling
axon development
cell junction assembly
axonogenesis
synapse assembly
Count
P adjusted
1e−11
2e−11
3e−11
B
mRNA expression across cell clusters
FOXG1
EMX2
Expression Level
ROSA26
ΔHS1332
ΔnMotif
Glutamatergic Neurons
Forebrain Progenitors
Peripheral Neurons
Neural Crest Precursors
Retinal Epithelia
Neural Progenitors
Retinal Neurons
Forebrain Neurons
Myelinating Cells
C
FACS-sorted rosettes
ROSA26
ΔHS1332
ΔnMotif
FOXG1/DAPI
PLZF/DAPI
SOX2/DAPI
50 µm
D
cerebral organoid formation
hESCs
cerebral organoids
E
cerebral organoids
Cerebral Organoid - 30 Days
Cerebral Organoid - 40 Days
ROSA26
ΔHS1332
ΔnMotif
GFP/DAPI
SOX2/DAPI
EMX1/DAPI
FOXG1/DAPI
NeuN/DAPI
TUJ1/DAPI
500 µm
1 mm

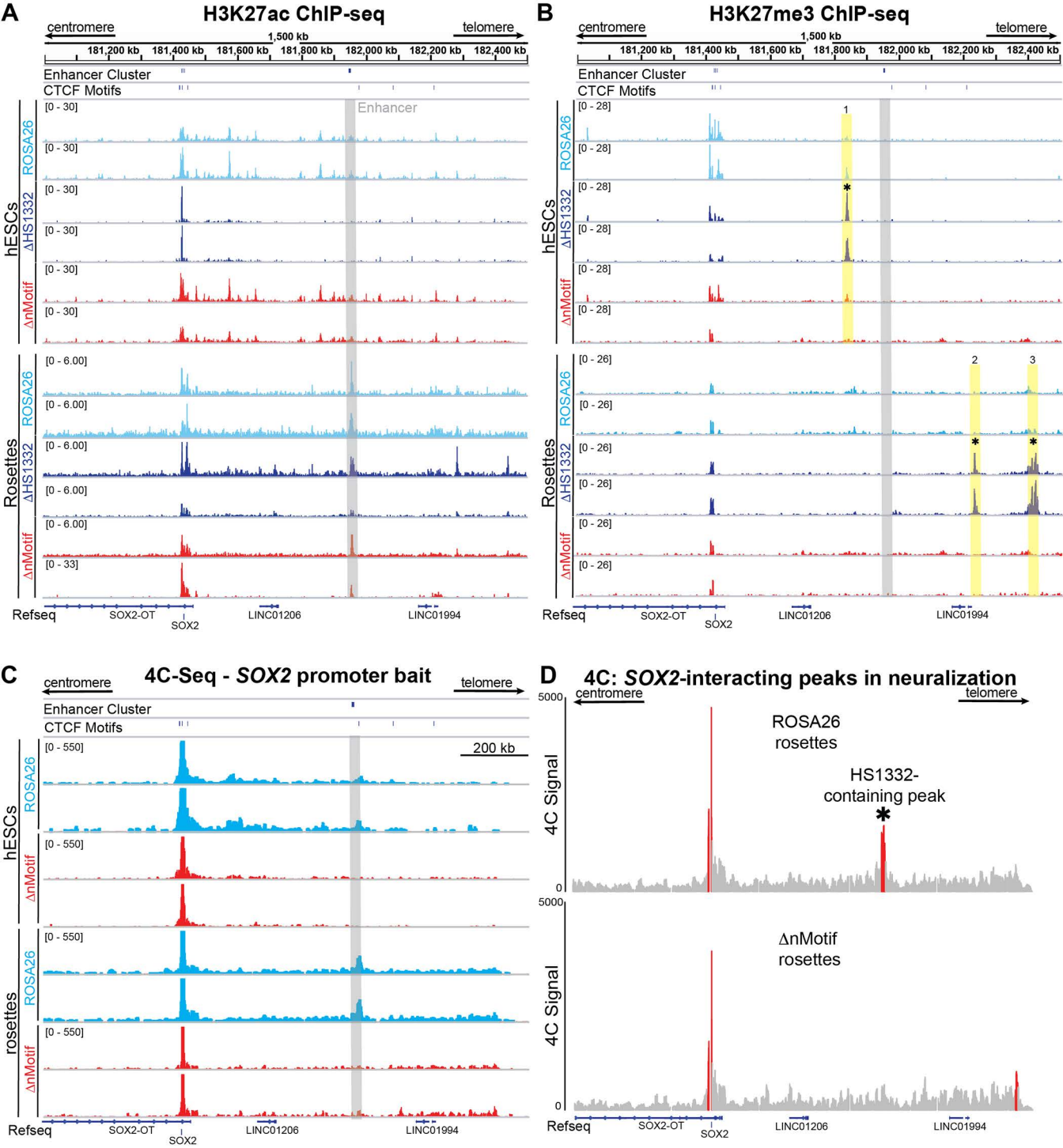
A
H3K27ac ChIP-seq
centromere
telomere
1,500 kb
181,200 kb
181,400 kb
181,600 kb
181,800 kb
182,000 kb
182,200 kb
182,400 kb
Enhancer Cluster
CTCF Motifs
Enhancer
hESCs
ROSA26
ΔHS1332
ΔnMotif
Rosettes
[0 - 30]
[0 - 6.00]
[0 - 33]
Refseq
SOX2-OT
SOX2
LINC01206
LINC01994
B
H3K27me3 ChIP-seq
[0 - 28]
[0 - 26]
1
2
3
C
4C-Seq - SOX2 promoter bait
200 kb
[0 - 550]
D
4C: SOX2-interacting peaks in neuralization
4C Signal
5000
0
ROSA26
rosettes
HS1332-
containing peak
ΔnMotif
rosettes

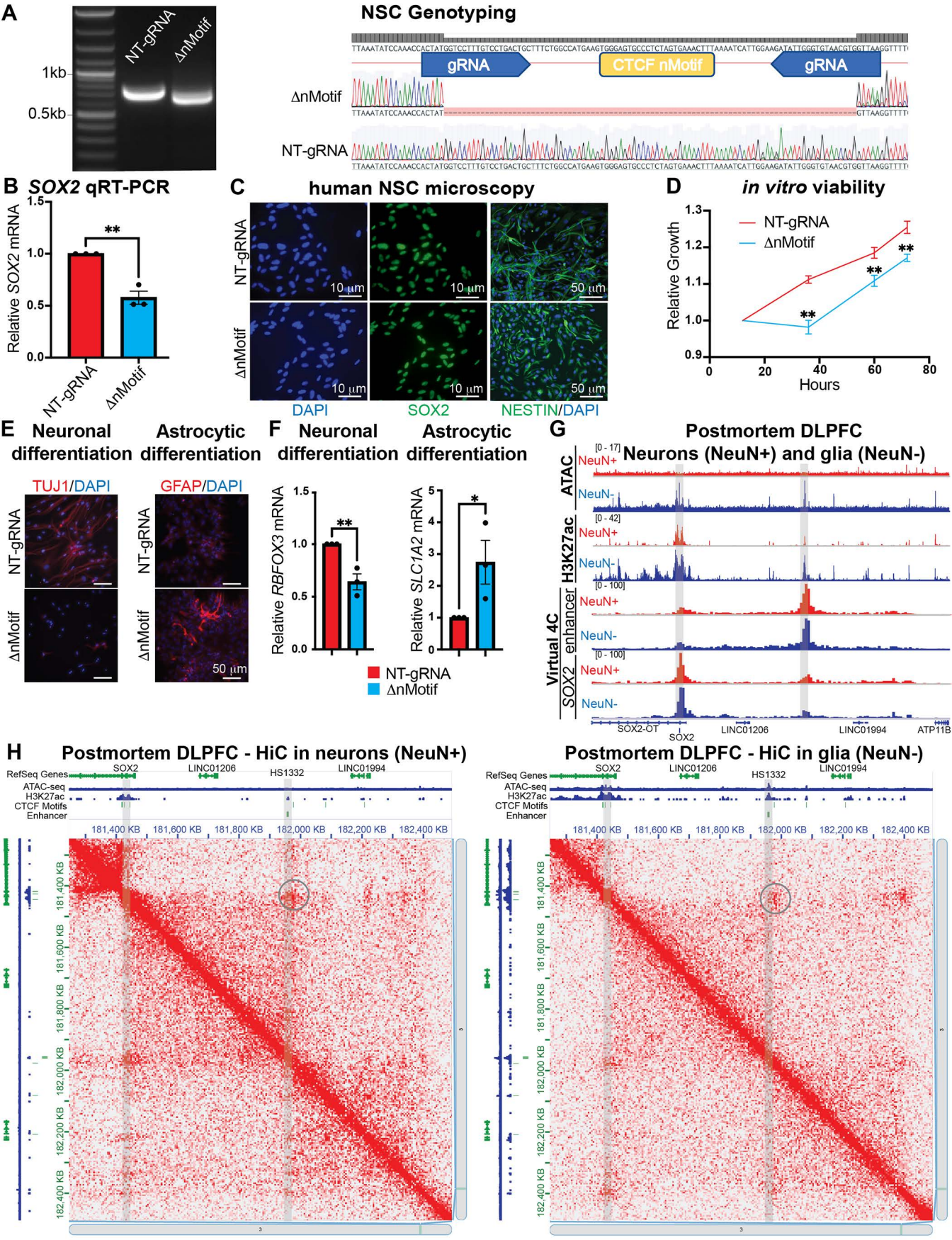
A
NT-gRNA
ΔnMotif
1kb
0.5kb
NSC Genotyping
gRNA
CTCF nMotif
gRNA
ΔnMotif
NT-gRNA
B SOX2 qRT-PCR
Relative SOX2 mRNA
NT-gRNA
ΔnMotif
C human NSC microscopy
NT-gRNA
ΔnMotif
10 µm
50 µm
DAPI
SOX2
NESTIN/DAPI
D in vitro viability
Relative Growth
NT-gRNA
ΔnMotif
Hours
E Neuronal differentiation
Astrocytic differentiation
TUJ1/DAPI
GFAP/DAPI
NT-gRNA
ΔnMotif
50 µm
F Neuronal differentiation
Astrocytic differentiation
Relative RBFOX3 mRNA
Relative SLC1A2 mRNA
NT-gRNA
ΔnMotif
G Postmortem DLPFC
Neurons (NeuN+) and glia (NeuN-)
ATAC
H3K27ac
Virtual 4C
enhancer
SOX2
NeuN+
NeuN-
SOX2-OT
SOX2
LINC01206
LINC01994
ATP11B
H Postmortem DLPFC - HiC in neurons (NeuN+)
Postmortem DLPFC - HiC in glia (NeuN-)
RefSeq Genes
ATAC-seq
H3K27ac
CTCF Motifs
Enhancer
SOX2
LINC01206
HS1332
LINC01994
181,400 KB
181,600 KB
181,800 KB
182,000 KB
182,200 KB
182,400 KB